Magnesiothermic Conversion of Sintered-Closely Packed Diatom (*Coscinodiscus wailesii*) Monolayer on Silicon Wafer and its Optical Properties.

by

Srisuda Rojsatien

A Thesis Presented in Partial Fulfillment
of the Requirements for the Degree
Master of Science

Approved April 2018 by the
Graduate Supervisory Committee:

Michael Goryll, Co-Chair
Terry Alford, Co-Chair
David Theodore

ARIZONA STATE UNIVERSITY

May 2018

ABSTRACT

The hierarchical silica structure of the *Coscinodiscus wailesii* diatom was studied due to its intriguing optical properties. To bring the diatom into light harvesting applications, three crucial factors were investigated, including closely-packed diatom monolayer formation, bonding of the diatoms on a substrate, and conversion of silica diatom shells into silicon.

The closely-packed monolayer formation of diatom valves on silicon substrates was accomplished using their hydrodynamic properties and the surface tension of water. Valves dispersed on a hydrophobic surface were able to float-up with a preferential orientation (convex side facing the water surface) when water was added. The floating diatom monolayer was subsequently transferred to a silicon substrate. A closely-packed diatom monolayer on the silicon substrate was obtained after the water evaporated at room temperature.

The diatom monolayer was then directly bonded onto the substrate via a sintering process at high temperature in air. The percentage of bonded valves increased as the temperature increased. The valves started to sinter into the substrate at 1100°C. The sintering process caused shrinkage of the nanopores at temperatures above 1100°C. The more delicate structure was more sensitive to the elevated temperature. The cribellum, the most intricate nanostructure of the diatom (~50 nm), disappeared at 1125°C. The cribrum, consisting of approximated 100-300 nm diameter pores, disappeared at 1150°C. The areola, the micro-chamber-liked structure, can survive up to 1150°C. At 1200°C, the complete nanostructure was destroyed. In addition, cross-section images revealed that the

valves fused into the thermally-grown oxide layer that was generated on the substrate at high temperatures.

The silica-sintered diatom close-packed monolayer, processed at 1125°C, was magnesiothermically converted into porous silicon using magnesium silicide. X-ray diffraction, infrared absorption, energy dispersive X-say spectra and secondary electron images confirmed the formation of a Si layer with preserved diatom nano-microstructure. The conversion process and subsequent application of a PEDOT:PSS coating both decreased the light reflection from the sample. The photocurrent and reflectance spectra revealed that the Si-diatom dominantly enhanced light absorption between 414 to 586 nm and 730 to 800 nm. Though some of the structural features disappeared during the sintering process, the diatom is still able to improve light absorption. Therefore, the sintering process can be used for diatom direct bonding in light harvesting applications.

DEDICATION

to all diatoms I have killed

to my father who always loves and supports me

to my mother who is waiting to cook all of my favorite foods for me at home

to my older sister for being my second mom

to my younger sister who makes me want to be a better sister everyday

to Izak, my boyfriend, the most beautiful distractor on earth

to my thesis advisor, Dr. Goryll, who believes in me

ACKNOWLEDGMENTS

First of all, I would like to thank my thesis advisor, Dr. Michael Goryll, for accepting me to be part of his research group, guiding me, teaching me, and encouraging me to be a better scientist. Next, I would like to thank Dr. Terry Alford for helping me find a research group when I first came to ASU and for helping me again in my last semester to find the remaining committee member. I am also thankful for Dr. David Theodore for being my committee member, and Dr. Zachary Holman I appreciate for allowing me to use the UV-Vis spectrometer in his lab.

Thesis (sometimes) is not about working alone by yourself. My research was done faster with technical help from Mr. David Wright (Goldwater Material Science Facility), Salman Manzoor (Dr. Holman's group) who trained me on the UV-Vis spectrometer, and Frank Tsang, my first ASU lab mate, who helped me with photoresist-treatment. Importantly, Dr. Martyn Fisher, who trained me on tools (the UV-Vis, FTIR and spin coater), proofread my work, and advised me on research and life.

My thought has been attached to the diatom structures since I was 17. My curiosity about the diatom has grown thank to my undergrad advisor, Dr. Surachai Thachepan, Department of Chemistry, Kasetsart University (Thailand) who allowed me to work on diatoms and invested in the *C.wailesii*. I also have to thank Dr. Jantana Praiboon and her master student, Mr. Panjaphol Chaisutyakorn, of Algal Bioresource Research Center, Department of Fishery Biology, Kasetsart University, who provided the cultivation medium and a controlled room for diatom cultivation.

Lastly, I would like to thank the National Science Foundation (NSF) and Fulbright for offering the financial support for my Masters study.

TABLE OF CONTENTS

Page

CHAPTER Page

CHAPTER Page

LIST OF TABLES

Table Page

LIST OF FIGURES

Figure Page

Figure Page

Figure Page

Figure Page

CHAPTER 1

INTRODUCTION

1.1 Motivation

Diatoms, the group of photosynthetic marine microalgae, have fascinating silica hierarchical structures (frustules) with quasi-ordered patterns of nano-micro pores. The silica nanostructures form without requiring extreme conditions of pH, temperature, and pressure. After millions of years of evolution, the diatoms are able to transport silicic acid from the environment through the cell membrane by molecular self-assembly[9] and phase separation processes[10]. Studies have revealed various functions of the structure. Not only does it protect against mechanical stress, animal grazing, and other noxious agents[11], but the diatom structure, especially that in Coscinodiscus genus, can also manipulate and exploit light, mainly to enhance photosynthesis performance. For example, *Coscinodiscus granii*'s frustules act as photonic-crystal slabs, which can confine photons coupled into the slab[12]. The confined light can be effectively used by chloroplasts located close to the cell walls[9]. Additionally, the studies of *Coscinodiscus wailesii* revealed that the frustules can act as a microlens[13] and confine the light[14] due to the superposition of the waves scattered by pores on the valves. Another study also demonstrates that the valves of *C. wailesii* are capable of redistributing the transmitted light and concentrating the light into certain locations[15]. Furthermore, the frustules of *C. wailesii* can enhance light absorption efficiency within the 400-500 nm and 650-750 nm region, and significantly manipulate the

incoming light by coupling into localized waveguiding modes, thus, increasing the solar energy conversion efficiency in the diatom[2].

Therefore, due to their appealing nano-micro structure and optical properties, silica diatom frustules were converted into silicon diatoms using a magnesiothermic conversion process. Additionally, since Si-nanostructures are used for solar energy conversion[16], [17] and energy storage[11], [18], converting SiO_2 diatoms into Si with preserved nano-structures may allow us to use the diatom frustules for those applications. The pioneer diatom conversion work was from Bao et al.[19], who used magnesium vapor from magnesium to convert silica diatoms at high temperature, with molar ratio of Mg: SiO_2 as 2:1. MgO was then selectively dissolved by 1M HCl. The Si diatoms were photoluminescent, and possibly used in microscale gas sensing. Though the converted nano-structure of the Si diatoms were well preserved, the vapor pressure from magnesium metal was high enough to drive the formation of magnesium silicide, Mg_2Si[20], which was an undesired product.

Luo et al. did a similar experiment but added NaCl as a heat scavenger. They found that SiO_2 diatoms were converted into Si-diatoms without the formation of Mg_2Si[21]. However, addition of NaCl may introduce Na defect to Si-diatoms, decreasing Si performance for photovoltaic applications. Furthermore, to avoid the formation of magnesium silicide, Chandrasekaran et al.[22] decreased the molar ratio of Mg to SiO_2 to 1.25:1. The diatoms were successfully converted into silicon with preserved structure. Boron-doped Si-diatoms were then used to fabricate a photocathode, which was able to produce hydrogen via photoelectrochemical reaction[23]. However, based on this

magnesiothemic conversion, some diatoms could not react with magnesium, since the magnesium amount was not equivalent to the silica amount.

In 2016, Liang et al. offered another path for magnesiothermic conversion. They converted SiO_2 diatoms into Mg_2Si/MgO diatoms using excess Mg vapor, then converted the Mg_2Si into Si/MgO composite via oxidation reaction[24]. Mesoporous Si-diatoms were used as an anode for lithium ion batteries. Nevertheless, the molar volume of Mg_2Si/MgO is significantly higher than that of SiO_2[25], causing the starting diatom structure to collapse after the oxidation and MgO-selective dissolution.

To completely convert SiO_2 into Si diatoms with well-preserved structure, Gordin used magnesium silicide as the magnesium vapor source instead of using magnesium metal[26]. With the lower Mg vapor pressure, SiO_2 diatoms were converted directly into Si without Mg_2Si formation, thus preventing the diatom structure from collapsing.

While the frustule properties and the conversion of Si-diatoms including their applications were thoroughly investigated, there were only a small number of studies trying to deposit a closely-packed diatom monolayer on substrates. The monolayer deposition is one of the critical factors, which enables the intriguing diatom structures to be used in real-world applications. Self-assembly of floating diatoms[5], [27], bubbles generated from heating water[6] , and N_2 bubbles induced agitation[7] were found to facilitate the diatom monolayer formation. However, those methods have limitations due to the orientation of diatoms, area of the monolayer, and reproducibility. Thus, more studies were needed to develop the closely-packed diatom monolayer formation.

Furthermore, there was little research focusing on bonding SiO_2 or, Si diatoms onto a substrate. Losic and et al. bonded diatom frustules with a polylysine-treated Si substrate[28]. The bond strength was not investigated and it is assumed be weak. Chandrasekaran et al. modified the surface of Si-diatom with organic thiols via hydrosilylation before attaching the thiol-modified Si-diatoms on Au-coated glass slides to fabricate a photocathode for water splitting[23]. Sulfur compounds may bind to Au surface via weak bonds (physisorption) or large van der Waals forces[29]. Nevertheless, using molecular linkage between the diatoms and the substrate creates an interfacial layer, which may form an insulating layer or scatter electrons in an electronic device. Thus, direct bonding between diatom frustules and a substrate without any molecular linkage may increase the probability of electrons transporting from the diatom frustule through the silicon substrate.

Pan et al. directly bonded SiO_2 diatoms on Si substrate at 75 °C, assisted by hydrofluoric acid (HF)[8]. The diatoms were bonded to the substrate via Si-O-Si bonding. Other than the fact that heating HF would create harmful vapor, this bonding process could not be used to bond Si diatoms on a substrate. Even if one wants to convert the bonded SiO_2 diatoms from this bonding process into Si-diatoms using magnesiothermic conversion, Si-O-Si bonding would be destroyed during the conversion process.

Although sintering processes at high temperature have been used to bond silica nano-particles on Si wafer substrates[30], [31], this process has not been used to bond SiO_2 diatoms on Si wafers due to the concern that the high temperature might destroy the

diatom structure[8] . However, there is no reported data concerning the highest temperature that the diatom structure can tolerate.

Therefore, in this work, the closely-packed diatom monolayer, bonding via sintering process, magnesiothermic conversion, and optical properties of the modified diatoms have been investigated.

1.2 Overview of this work

A new method for assembling closely-packed diatom monolayers with a preferable orientation was investigated. A sintering process at high temperature was examined as an alternative approach to directly bonding the diatom monolayer on a Si substrate. The bonded SiO_2 diatoms on the substrate were then converted into Si-diatoms via magnesiothermic conversion, using Mg_2Si as the Mg vapor source. Next, the Si-diatoms on the substrate were spin-coated with Poly(3,4-ethylenedioxythiophene): polystyrenesulfonate (PEDOT: PSS), a highly conductive polymer with relatively high work function[32], to provide a hole collector layer and improve the optical properties. The optical and electrical properties of PEDOT:PSS coated Si-diatoms on the substrate were investigated using reflectance spectrometer and photocurrent measurements.

CHAPTER 2

THE CHOSEN DIATOM *(Coscinodiscus wailesii*) AND ITS MORPHOLOGY

2.1 Introduction

Diatoms, a group of unicellular algae containing approximately tens of thousands of species, are a predominant natural source of silica nanostructures. They provide various silica nanostructures since each of them possesses a unique silica morphology of their cell wall (frustule) as shown in Fig.2-1. The diatom structures are reproduced by cell division with high fidelity as the division process is genetically controlled. Moreover, the silica structure is formed without requiring extreme conditions of pH, temperature, and pressure. After millions of years of evolution, the diatoms are able to transport silicic acid from the environment through the cell membrane, using a group of proteins called silicic acid transporters. Within the cell, the silicic acid is then transported to silica deposition vesicle (SDV), where silica polymerization occurs. The polymerization of silica from silicic acid produces micro silica particles. The size and properties of these particles depend on pH and the presence of salts. The movement of SDV during silification control the formation of the larger scale structure. SDV thus serve as a mold for structural formation of the diatoms [33].

The functions of diatom frustules, particularly mechanical protection and light manipulation for photosynthesis, have been revealed in various studies. Hamm et al. studied the mechanical strength of centric diatoms (*Coscinodiscus granii* and *Thalassiosira punctigera*) and a pennate diatom (*Fragilariopsis kerguelensis*) using calibrated glass

microneedles and finite element analysis. The measurement revealed that these frustules are remarkably strong due to their architecture. Thus, the silica structures may provide themselves the mechanical protection against predators [34].

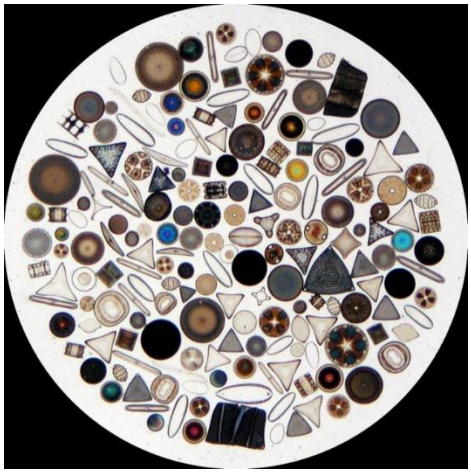

Figure 2-1 Various shapes of diatom frustules[1]

Furthermore, light manipulation for photosynthesis performance was studied as another function of diatom frustules. The periodic hierarchical structure of *C. granii* acted as photonic-crystal slabs, which can confine coupled photons in the visible range into the slab[12]. The confined light could be effectively used by chloroplasts, located close to the cell walls[9]. A study of *Coscinodiscus wailesii,* another centric diatom with a periodic hierarchical structure, revealed that the frustule could act as a microlens. A petri-dish like frustule of the *C.wailesii* is composed of two valves which are joined by girdle bands. The frustule narrowed a red laser beam from a 100 μm spot size to 10 μm when the beam was transmitted through the diatom structure. Numerical simulations of the electromagnetic field propagation demonstrated that the focusing effect was due to the superposition of the

waves scattered by pores on the diatom valve [13]. Moreover, it was found that dimension of the confined light depended on the wavelength of the incoming light. Based on the simulations, the valve could not confine ultraviolet light which is harmful for living organisms and not useful for photosynthesis. This reveals a possible evolutionary advantage of the diatom structure [14].

The light transmission through individual valves of *C.wailesii* frustule was further investigated by Hsu et al [15]. Cross-sectional intensity profiles of transmitted light showed that the valves could redistribute and concentrate the transmitted light into certain locations. They found that, when the distance between the light source and the valve was shorter than the valve diameter, the transmitted light was concentrated at the center of the valve. When the distance was longer, the transmitted light showed ring-shape profiles. The distances, which caused the center- and ring-concentrated profiles, were inversely proportional to wavelengths of the incoming light.

In addition, the light trapping effect of *C. wailesii* frustule was studied using Rigorous Coupled Wave Analysis (RCWA) and the Finite-difference time-domain (FDTD) method [2]. It was found that the frustule enhanced light absorption efficiency at 400-500 nm and 650-750 nm region, which agreed with the experimental results as shown in Fig. 2-2.

It has been proven by a number of studies that the *C. wailesii* frustule, as a natural biosilica structure, possesses intriguing optical properties. The diatom is therefore used in this study.

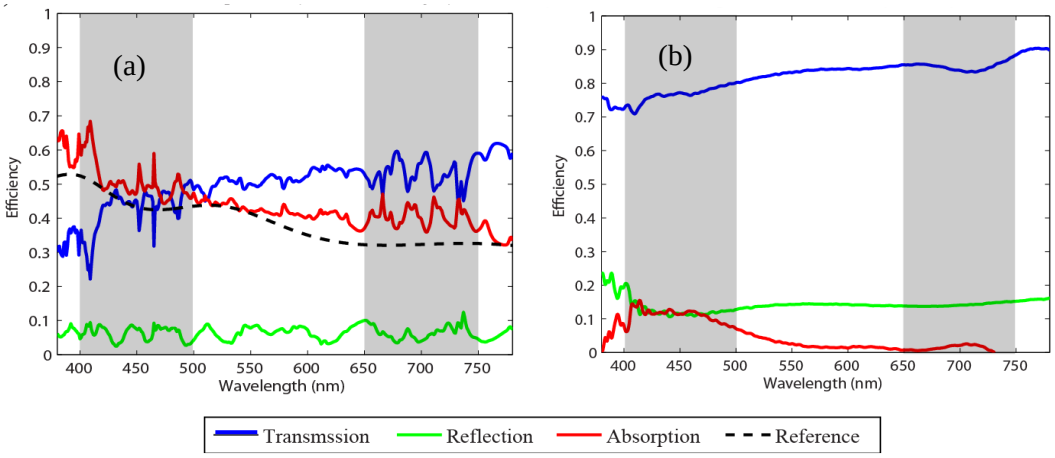

Figure 2-2 Simulated and experimental spectra of the diatom. Spectrum generated by RCWA simulation of the diatom model (a). The dashed curve in (a) is the spectrum of the reference model (a plane without pattern). The spectra of the diatom also experimentally obtained by optical spectroscopy (b) [2].

2.2 Diatom frustule preparation

The C.wailesii culture (CCMP2513) was purchased from the National Center for Marine Algae and Microbiota (NCMA, USA) by Asst. Prof. Surachai Tachepan, Department of Chemistry, Kasetsart University, Thailand. f/2 medium for the diatom cultivation was kindly provided by Dr. Jantana Praiboon from Algal Bioresources Research Center, Department of Fisheries, Kasetsart University, Thailand. 30% w/t hydrogen peroxide solution (H_2O_2) was provided by Asst. Prof. Tachepan.

The cultivation of *C.wailesii* diatom (Fig. 2-3) was carried out at the Algal Bioresources Research Center. The diatom was cultivated in f/2 medium[35] at 25°C under fluorescent light at 26-30 μmol·photons·m^{-2}·s^{-1} and continuous air. After cultivating for 20 days, the diatoms were stored in the dark for 24 hours to let them sink to the bottom of the

culture container. The upper part of the medium solution was removed using a siphon. The diatom cells were filtered from the rest of the medium solution using a plankton net with a maze size of 40 μm. The diatoms were then washed with distilled water 4 times. In order to remove the organic materials from the biosilica of the diatom, the aliquot of wet diatom (2g) was digested with 100 ml of 30wt% aqueous hydrogen peroxide at pH 2 in a 250-mL flask at 80°C for 24 h, and the solution was continuously mixed by magnetic stirrer[36]. The digested diatom frustules were settled at room temperature for 24 hours before the supernatant was removed by siphon. The frustules were washed with distilled water 4 times and then 1 time with ethanol by centrifugation at 2500 rpm for 10 min, until the pH was neutral. The frustules were stored in a vial and then dried at 80°C in an oven.

The morphology of the organic-free diatoms was investigated using secondary electron microscopy (SEM) on a XL30 environmental scanning electron microscope (ESEM) FEG and a Phenom World SEM.

Figure 2-3 The cultivation of *C. Wailesii*. The diatom cultivation in a 75-ml flask (left) which was then transferred into 1000-ml container (right) to increase the diatom production. The diatom cells can be seen as small brown particles floating in the medium.

2.3 Diatom Morphology

The morphology of the cleaned diatoms from section 2.3 was investigated using Scanning Electron Microscope (SEM). The petri-dish like *C.wailesii* cell is composed of two flat valves joined together by girdle bands (Fig. 2-4a). A valve (~100 μm in diameter, ~0.9-1.4 μm thick) has a radial symmetry *(the radial arrangement of the pores around the valve center)* and hexagonal symmetry (porous pattern). A valve can be considered as the superstition of inseparable-three layers (Fig. 2-4f). The external surface layer of the valve (cribrum) has flower-liked groups of nanopores (~100-300 nm) connected to each other by a complex silica network (Fig. 2-4b-c). The pores of cribrum are closed by small sieve plates called a cribellum, resulting in nanopores (~50 nm) within the pores of cribrum (Fig. 2-4d). The middle layer is a chamber-like structure called areola which is consists of walls perpendicular to the cribrum (~0.3-0.5 μm height) (Fig. 2-4e). These walls of areola create cavities in the valve (~1.1-1.8 μm wide). The internal surface layer called foramen has a hexagonal array of micro-pores (~0.9-1.7 μm) (Fig. 2-4g). Each pore of foramen centers with both a cavity of areola and the flower-liked groups of nanopores in cribellum. From the internal surface side, the group of nanopores can be seen inside the foramen pores (Fig. 2-4h). The nanopores (~160μm) of a girdle band are shown in Fig. 2-4i.

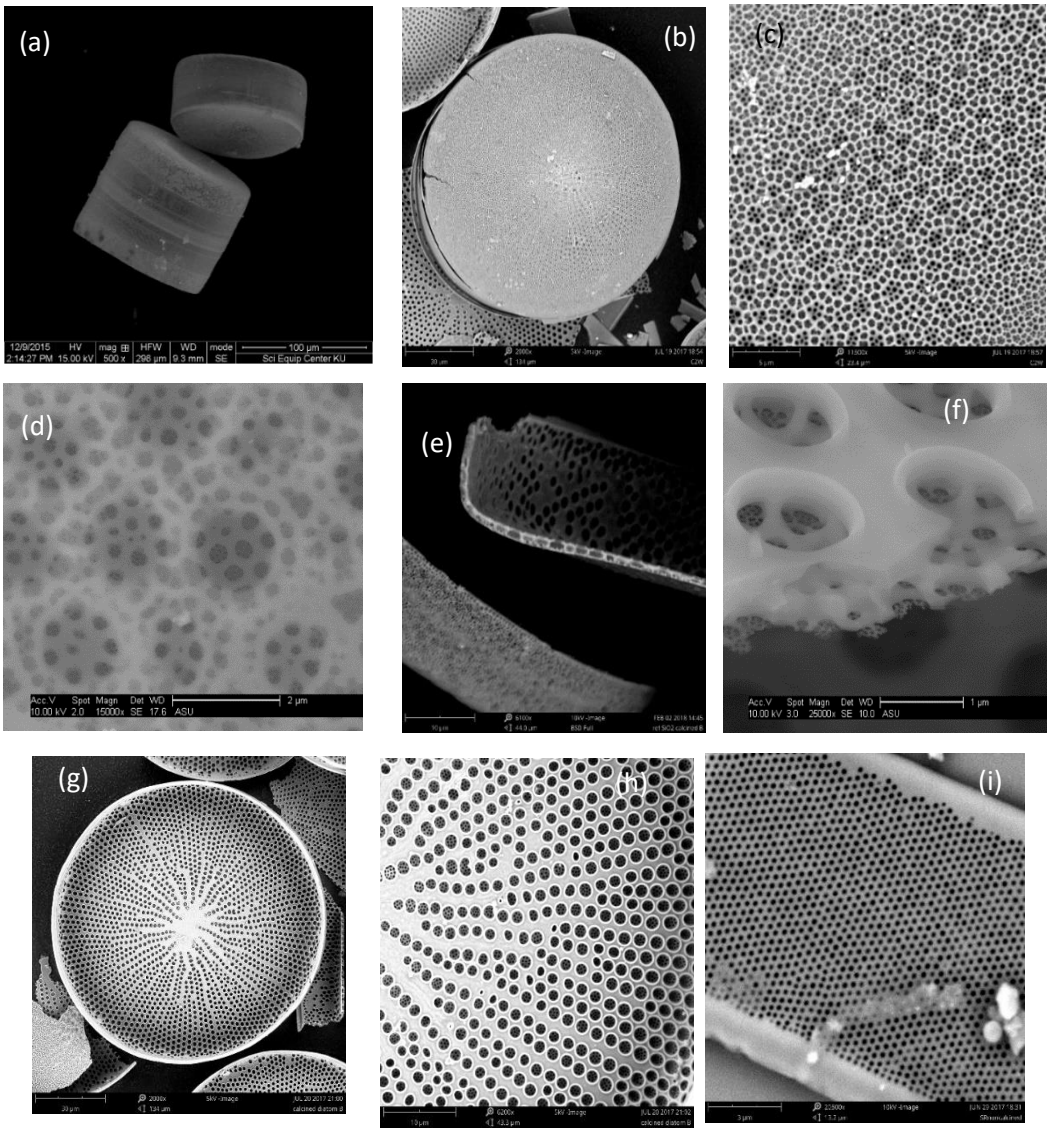

Figure 2-4 Secondary electron images of *C.wailesii* morphology: A C.wailesii's cell composed of two valves joined by girdle bands (top right, a). The external surface layer, cribrum (b), shows flower-liked groups of nano pores (~100-300 nm) connected by a complex silica-network (c). All pores of cribrum are closed by small sieve plates called a cribellum (d). A cross-section image of a valve reveals the cavities created by areola, the structure of walls perpendicular to the external surface (e). The other cross-section image shows that all layers of a valve are connected and inseparable (f). The internal surface layer (foramen) shows radial symmetry of micro-pores (g). Inside the foramen pores, the groups of nano-pores can be seen (h). The nanopores (~160μm) of a girdle band is shown in (i).

2.4 The formation of each valve

A valve formation of *C.wailesii* is an intriguing process comprised of three stages: development of the base layer, development of the areolae walls, and development of the outer layer, respectively [3]. In the first stage (the first horizontal differentiation), silicified strands are elongated and radiated from the center of the diatom (Fig. 2-5a). During the elongation, these strands start branching. Adjacent branches elongate to each other before they fuse and then form the base of areola (Fig. 2-5b). The second stage (vertical differentiation) is the growth of areole walls, transforming an irregular round outline at the base (Fig. 2-5c) to a hexagonal outline at the distal side (Fig. 2-5d). This stage is completed when the periodically-spaced vertical teeth with a particular height then form on top of the walls (Fig. 2-5e). The last stage (the second horizontal differentiation) is the formation cribrum and cribellum. The teeth horizontally grow toward the middle of each areola (Fig. 2-5f) and then become cross netted, resulting in a convex cribrum (Fig. 2-5g). Consequently, cribellum start to form at the cribrum locating above the internal foramen (Fig. 2-5h). Cribellum can grow further to close all pores of cribrum (Fig. 2-5i).

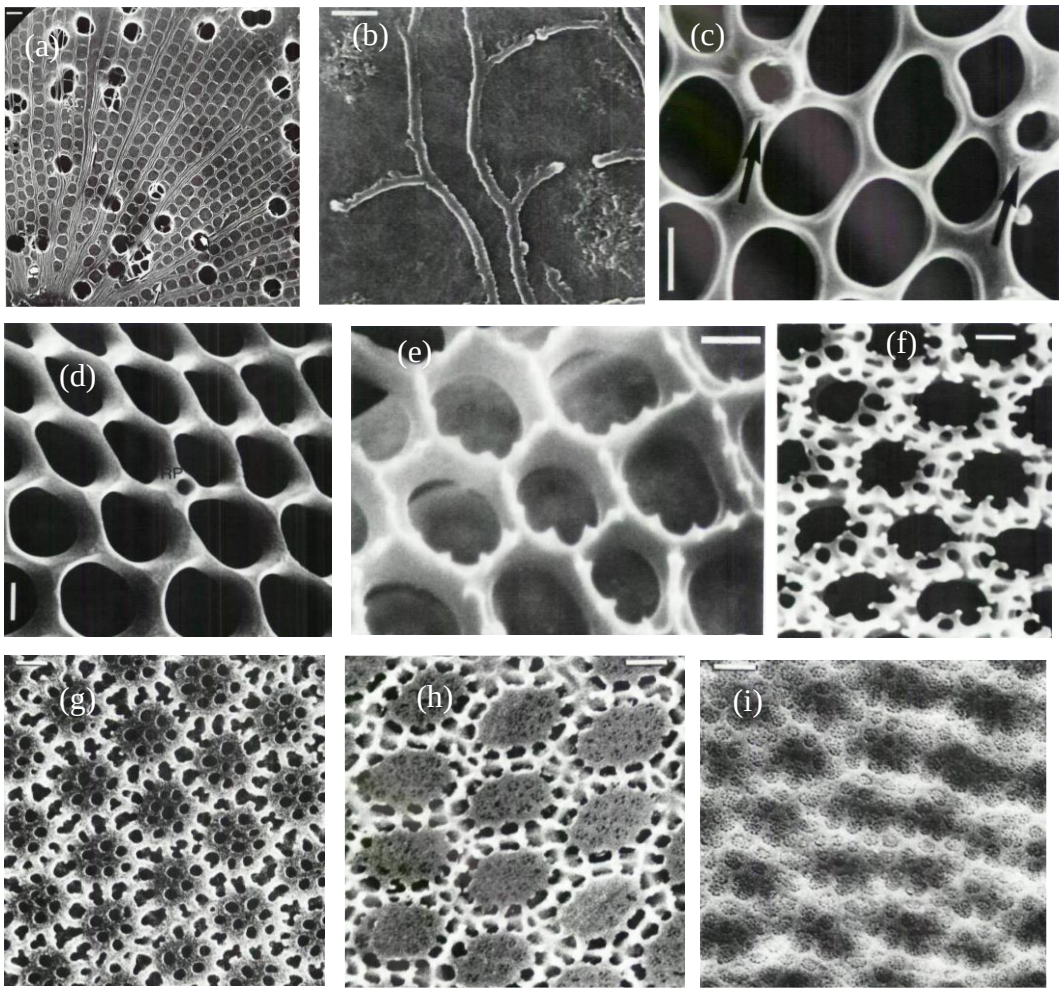

Figure 2-5 The formation of a valve of *C.wailesii.* It begins with the first stage: base layer formation (a and b). The second stage is the formation of areola (c-e). The last stage is the formation of cribrum (f and g) and cribellum (h and i) [3]. For the scale bar: (a) is 2 μm, (b) is 0.5 μm, and the rest is 1 μm.

CHAPTER 3

CLOSELY-PACKED MONOLAYERS OF THE DIATOM

3.1 Introduction

Due to its appealing optical properties and biosilica nanostructure of a single diatom in the Coscinodiscus genus, there are researches trying to form closely-packed monolayer of the diatoms on a substrate for various applications.

In 2012, Wang et al. studied the floating assembly of *Coscinodiscus sp.* After adding the organic-free and dried diatoms onto a water droplet, the diatom valves floated and assembled together at the top of the droplet (Fig. 3-1a). The closely-packed monolayer of the valves was formed on a glass surface after the water was evaporated and was bonded to the substrate using hot melt adhesive (HMD) as illustrated in Fig. 3-1a. The SEM image of the fixed valves on the substrate is shown in Fig. 3-1b. The convex shape and the 40 nm-sieve pores on the valve external surface (Fig. 3-1d) facilitated the floating process, while the buoyancy and micro-range attractive forces (Fig. 3-1c) were responsible for the self-assembly at the top of the droplet. Furthermore, it was found that the valves sank when they were turned over, their sieve pores were enlarged using hydrofluoric acid (HF), the surface tension of water was reduced, or the valves were vacuumed by pumping. The authors proposed that the fixed valve monolayer on the substrate would be valuable for diatom-based devices such as biosensors, solar cells, and batteries[4].

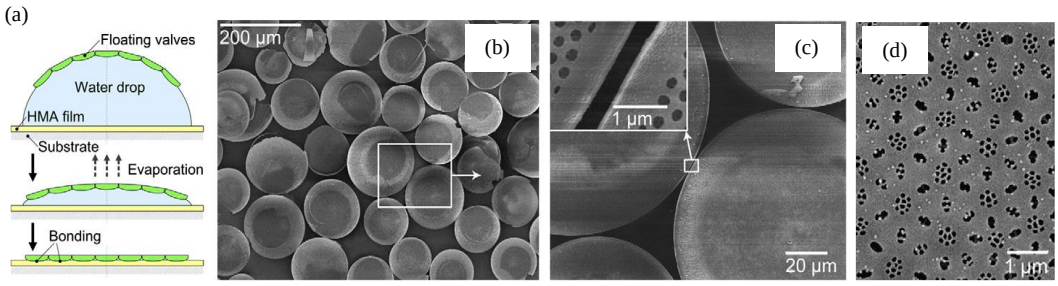

Figure 3-1 A schematic diagram (a) and SEM images of the floating self-assembly process to form a monolayer of valves on a glass substrate The SEM images show the monolayer valves which were fixed on the substrate using HMA. The micro-range attractive force was evident in (c) as the small gap between the adjacent valves was in micro-range. The sieve pores on the external surface of the valves was shown in (d)[4]**.**

Although the above method is simple and effective, the production of the monolayer with large area was not investigated. Kwon et al. thus introduced a new method to produce the monolayer of *Coscinodiscus sp.* valves with large area[5]. In their work, the diatoms were dispersed in ethanol before they were carefully transferred to the wafer surface. The ethanol decreased surface tension of the water, allowing the diatom valves to move at the surface and form a semi-ordered assembly using attractive capillary force between the valves. To produce a closely-packed monolayer, the surfactant Triton X100 was used as it has no charge to disturb the monolayer. Importantly, the surfactant provided surface pressure to the raft of the floating valves and pushed them together [37], [38]. The UV-curable polymer NOA60 coated substrate (silicon wafer) was lifted up across the water-air interface to collect the monolayer valves as illustrated in Fig. 3-2a. It was observed in this work that the lift rate was a critical factor. It had to be fast enough to avoid the separation of the monolayer film but had to be slow enough to allow the valves to

adhere to the surface. They found that the optimum rate was 0.5 mm/s. The obtained monolayer with large area is shown in Fig. 3-2b. An SEM image (Fig. 3-2c) revealed that the transferred monolayer film was a hexagonal-closely-packed monolayer with few voids and multilayer stacking. The SEM image with a higher magnification (Fig. 3-2d) showed that edges of some valves were overlapped with each other. They found that the orientation of the diatoms was both convex and concave sides.

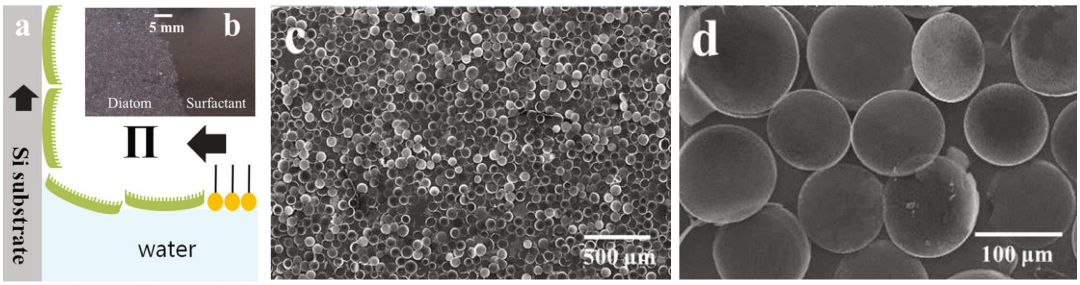

Figure 3-2 A schematic diagram demonstrating the production of a closely-packed monolayer of the diatom valves on the substrate (a). The valves were represented as the green boat-liked structure. The Triton X100 was represented by the pin-liked structure with a yellow head. A micrograph of the floating monolayer on the water is shown in (b). The wide view of the monolayer on NOA60 coated substrate is shown in (c). It reveals multi-stacking and voids in the film. A higher magnification of (c) is shown in (d)[5].

Moreover, the assembled diatom on the substrate was functionalized with gold. Thin gold film on the diatom surface enhanced Surface Enhanced Raman Scattering (SERS) by the factor of $2x10^4$ while small gold particles attached to the diatom surface enhanced the SERS by the factor of $7x10^4$ because of stronger localization of surface plasmons[5].

In 2015, Cai et al. developed another method to from a closely-packed monolayer of *Coscinodiscus sp.* valves. The organic-free and dried valves were added into water with high concentration. The valve solution was then pipetted onto a silicon wafer. The wafer

was quickly evaporated by heating the sample to the boiling point of water, resulting in a concave-up self-assembled monolayer of the valves (Fig. 3-3a and Fig. 3-3b). On the other hand, the self-assembly showed the mixed orientation of the valves (concave-up and -down) when the water was slowly evaporated at room temperature (Fig. 3-3c and Fig. 3-3d). It was explained that the bubbles, which were created during the fast evaporation, disturbed the valve orientation and thus caused them to orient in the more stable orientation, the concave-up. This hypothesis was supported by the control experiment which allowed the water to slowly evaporate at room temperature. The control showed that, without any distribution, the concave-up and down orientation were nearly equal[6].

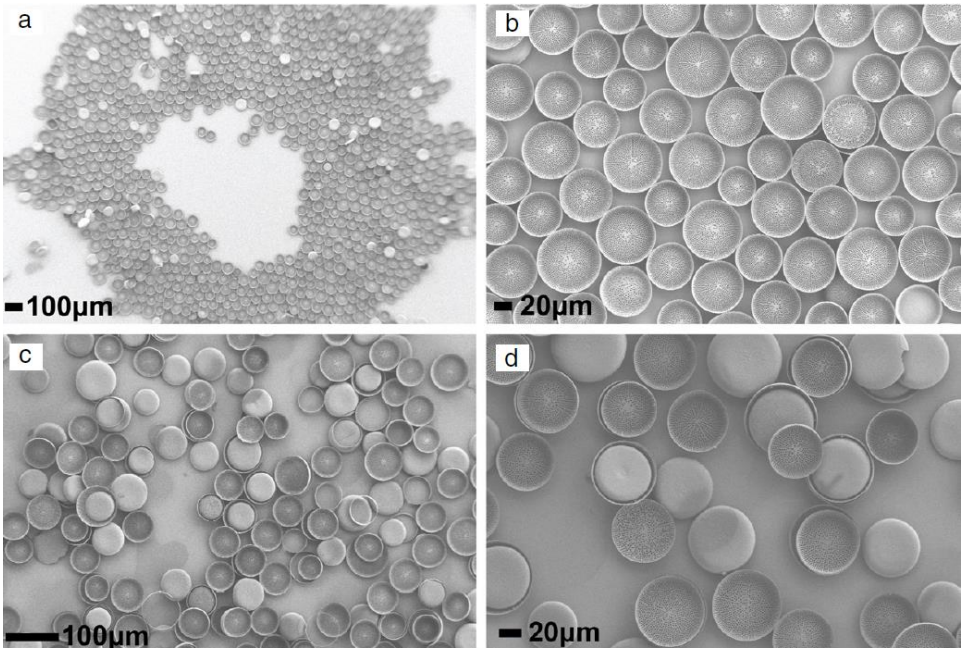

Figure 3-3 The diatom valve manipulation with fast (a and b) and slow evaporation (c and d). The former shows uniform concave-up orientation while the latter shows the overlapped valves with the both concave-up and down[6]**.**

In 2016, Li et al. demonstrated another method leading to a closely-packed monolayer of *Coscinodiscus sp.* with a uniform orientation and larger area. The organic-free valves were firstly modified with NXT-110 mold release agent in order to make the valves more hydrophobic. The authors suggested that the hydrophobicity of the valves would allow them to float on top of water in a water bath. The uniform orientation of the floating monolayer was obtained by bubble (N_2 gas)-induced agitations. 10% sodium dodecyl sulfate-water solution was used to push the valves together in order to form the closely-packed monolayer. The monolayer film was lifted up by a round cover slide. It was found that nearly 90% of the valves were oriented into concave down by bubble-induced agitation method (Fig. 3-4). The analytical study and simulations revealed that the agitation caused the valves to temporary submerse under the water surface. During subsequent rising toward the water surface, the valves adjusted their orientation into the ultimately favor one, the concave-down[7].

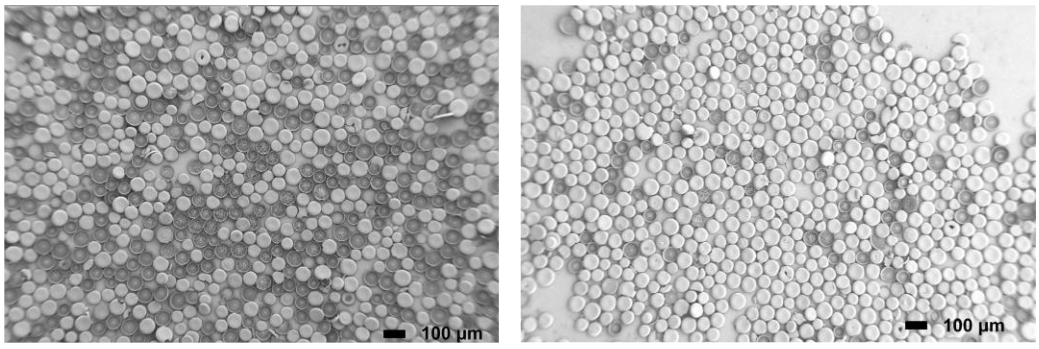

Figure 3-4 The orientation of a closely-packed monolayer without (left) and with bubble-induced agitation method. The latter shows nearly 90% of concave-down orientation[7].

Although the bubble-induced agitation method provided the closely-packed monolayer with large area and mostly-concave-up orientation, the method may not be suitable for the aims of the thesis as the concave-down orientation would provide less contact area between the valves and a substrate. This would lead to less efficient bonding between the diatoms and the substrate as the ring shape contact area provided by the concave-down would lower the probability that a valve can bond to the substrate. In this thesis, the concave-up orientation is thus highly preferable. The previous methods from Wang et al (2012) and Cai et al (2015) are considered as they provided the closely-packed monolayer diatoms with concave-up orientation. However, it was found in a preliminary experiment of this thesis that the *C.wailesii* valves were not able to float on top of a water droplet as reported in Wang et al (2012). The valves sank after they were added on top of the droplet. Moreover, in another preliminary experiment, the method provided by Cai et al (2015) could not produce a closely-packed monolayer of *C.wailesii.*

Therefore, a new method, which was adapted from Wang et al (2012), was developed in this thesis. Instead of adding dried valves on top of a water droplet, a water droplet was added on top of the valves which were dispersed on a hydrophobic substrate. The monolayer formation was investigated by optical and scanning electron microscopes.

3.2 Materials and Method

3.2.1 Separation of girdle bands from valves

The girdle bands were separated from the valves via a procedure adapted from the settling method[39]. 5 mg of the dried frustules were mixed and fully stirred with 50 mL distilled water in a 50mL- centrifuge tube. The mixture was held still for 20 min, then the mixture above the 5-mL scale mark was removed into another container using a pipette. Distilled water was added into the centrifuge tube up to the 50-mL scale mark for the next repeated separation. The separation process was repeated 4 times. After the last separation, the diatoms settled at the bottom of the tube by gravity. The remaining water above the valves was gently removed by a pipette. The diatoms were dried at 80°C using a hot plate.

3.2.2 Diatom closely packed monolayer

This process was performed in a small room with a HEPA air filter to minimize the dust contamination of the samples, preventing small particles, which may interrupt the contact between the diatom valves and the silicon wafer. Silicon wafers used in this process were spin coated with photoresist before they were cleaved by diamond pen into 1x1 cm^2 pieces. The purpose of the photoresist coating is to protect the silicon wafer's surface from silicon particle produced during the cleaving process, reducing obstacles for the diatom valve/silicon wafer bonding. The photoresist was then dissolved in an acetone/isopropanol solution.

The dried valves from the separation process were transfer to a Nylon cell strainer with 40 μm-maze size (Fisher Scientific, USA) and then washed with particle-free distilled water to remove small contaminant particles and debris from the valves. After the valves were dried at room temperature, they were dispersed on top of a hydrophobic surface

(PETE). 200 μL of particle-free distilled water was dropped on top of the dispersed valves, causing the valves to float up to the top of the water droplet and from a monolayer. The monolayer was collected by gently inserting a piece of the prepared silicon wafer under the monolayer (in the middle of the droplet) and quickly lifting up. The silicon wafer can still hold a smaller droplet of the water with the monolayer on top of it. Triton X-100 (Sigma Aldrich, USA) was used to make the diatom monolayer more compact[5]. After the water was dried at room temperature, the closely-packed monolayer of the diatom valves was deposited on the silicon wafer.

3.3 Results and Discussion

3.3.1 Separation process

The valves were separated from girdle bands using the settling method[39]. According to this method, the settling velocity of valves was faster than that of girdle bands, causing the valves to settle at the bottom of the tube while the girdle bands still remained suspended in the water. It was observed that the separation would not be successful if the concentration of the diatom in water was too low. The successfully separated valves (before filtration) and girdle are shown in Fig. 3-5a and Fig. 3-5b, respectively. Before filtration (Fig. 3-5a), the valves were contaminated with small debris, which could disrupt the valve/substrate interface during the sintering/bonding process. The debris was filtered by Nylon mesh filtration. The valves without debris are shown in Fig. 3-7a and Fig. 3-8.

3.3.2 Diatom closely packed monolayer

After the particle free distilled water was dropped on the dispersed valves, the valves floated up quickly and gradually assembled at the top of the water droplet, which can be seen as a white raft (Fig. 3-6). An optical image of the floating filtered valves is shown in Fig. 3-7a. The valves floated due to buoyancy and high surface tension of water as explained by Wang et al.[4]. In their work, they added another Coscinodiscus diatom on top of a water droplet without separating girdle bands from valves, as they found that the girdle bands would sink to the bottom. In this work, however, adding valves on a water droplet caused the valves to sink and the girdle bands needed to be separated from the valves as they could float on the droplet and disrupt the closely-packed monolayer formation (Fig. 3-7b). Moreover, it was observed that soaking non-floating valves in a water droplet and letting them dry at room temperature for 3-4 days, would allow those valves to float after a new water droplet was added on. It was also found that heated valves could not float. Thus, water vapor trapped in the valve structure may also contribute to the floating mechanism.

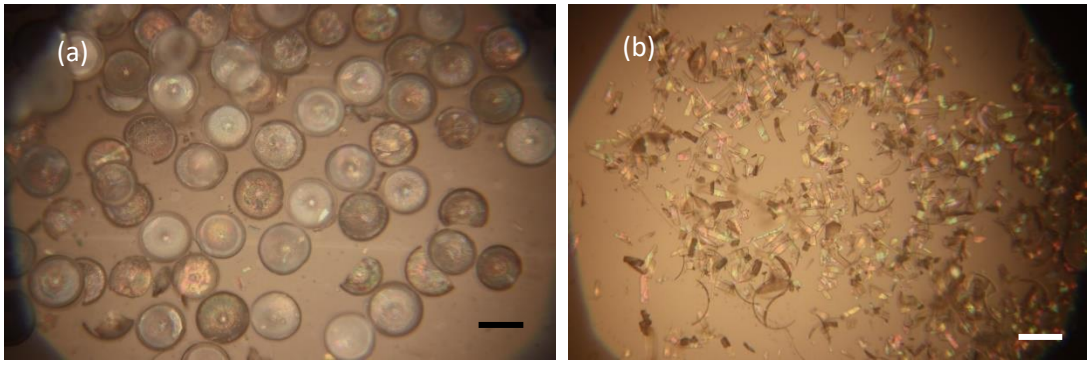

Figure 3-5 Separated valves before filtration (a) and separated girdle bands (b). The scale bar is 100μm.

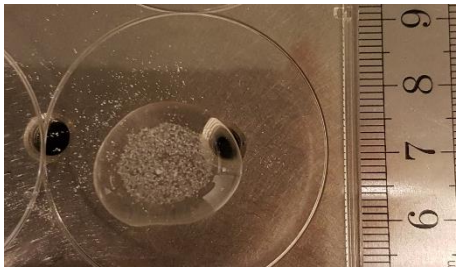

Figure 3-6 A photograph of the floating diatom monolayer on top of the water droplet. The floating monolayer can be seen as a white raft.

The self-assembly of the monolayer can be explained as the result of the balanced of force between the attractive force (bringing the valves together) and repulsive force (preventing the valves from severe aggregation in disordered state) [5]. A capillary attractive capillary force is generated by the deformed water surface caused by the diatom weight, which creates a negative meniscus at the valve surface. For repulsive force, the difference of the dielectric constants across the air-water interface generates an asymmetry charge distribution, which repels similarly-charged diatom valves[40]. The repulsion is a short-ranged force and only prevents the severe aggregation of the valve at the water surface. This allows the self-assembly process to reach highly-ordered equilibrium[5].

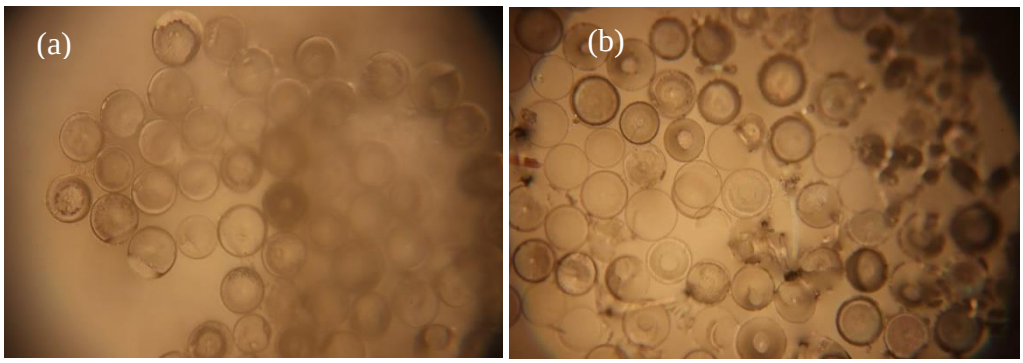

Figure 3-7 Optical images of a floating monolayer of valves without (a) and with girdle bands or debris (b) Noted that the valves (a) were filtered with the Nylon mesh to remove debris.

The Triton-X100 surfactant was added to make the arrangement of the valve monolayer more compact. The surfactant provided surface pressure to the raft of the floating valves and pushed them together [37], [38], making the monolayer more compact (closely-packed monolayer valves).

After the water was evaporated at room temperature, the closely-packed monolayer of the valves was deposited on the substrate, as observed with an optical microscope (Fig. 3-8a). The optical image with higher magnification (Fig. 3-8b) reveals that the orientation of the valves is mostly concave-up (or convex-down, external surface was in contact with the substrate), implying that the convex side was floating on the water surface. The convex-down orientation was able to float better than the concave-down, because the nanopores on the convex side prevented water from penetrating the structure and sinking the diatoms. On the other hand, the floating valves with the concave side on the water surface would have a higher tendency to sink, because more water would penetrate the structure through the micro-pores on the concave side [4]**.** The convex-down is the preferred orientation for the bonding process as it provides a high contact area between the valves and the substrate, enhancing the chance for the diatoms to bond to the surface.

Moreover, the larger circular monolayer area with a diameter up to approximately 1 cm (Fig. 3-9) was achieved by either using more dispersed valves or transferring the floating valves from one droplet to another using a silicon wafer piece. However, some valves started to overlap when the monolayer area was larger.

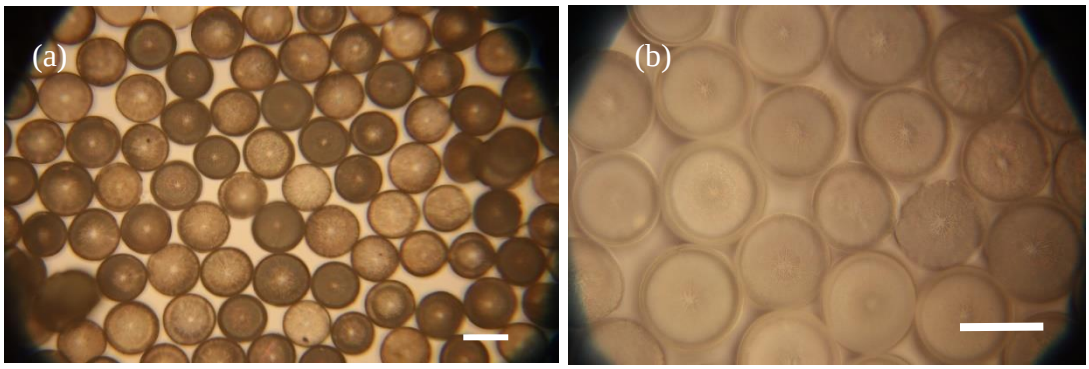

Figure 3-8 An optical image of a closely-packed monolayer of valves (a) and an image with higher magnification, revealing a monolayer with convex-down (concave-up) orientation (b). The scale bars are 100 μm.

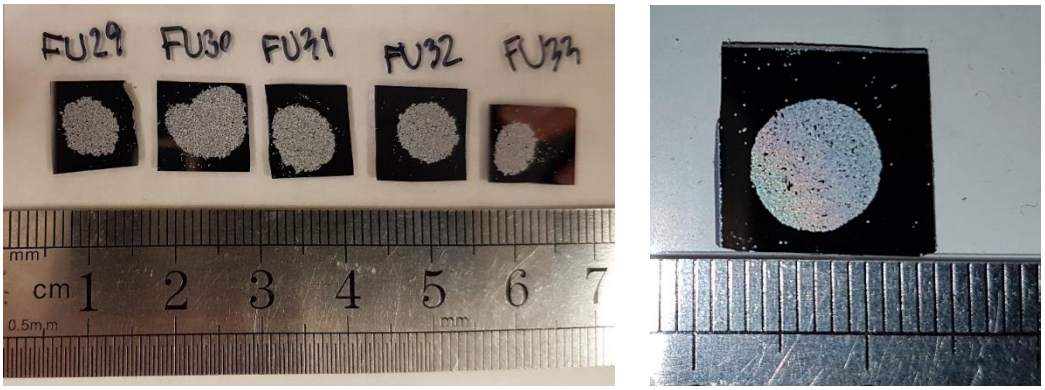

Figure 3-9 The photographs of the diatom monolayer on silicon wafer substrates. The large area monolayers were achieved based on the floating-up method. The right image shows iridescence of the large area monolayer.

In addition, it was observed that the floating properties of the valves changed when they were converted into Si-diatoms. Thus, it is easier to form closely-packed monolayer of SiO_2 diatoms before converting the SiO_2 diatoms into Si-diatoms. Additionally, the monolayer of SiO_2 diatoms needs to be strongly bonded onto the substrate to prevent the diatoms from detaching or being washed away from the substrate during the conversion process.

3.4 Conclusion

A monolayer of diatom valves was deposited on a silicon wafer substrate using floating properties of the valves and high surface tension of water. The valves floated up when water droplets were added on top of the dispersed valves on a hydrophobic surface. The valves sank, on the other hand, when they were added on top of a water droplet. Water vapor trapped inside the valve structure may play a crucial role for the floating behavior of the valves. Debris and girdle bands can disturb the monolayer formation. Based on this floating-up method, the formation of a closely-packed diatom monolayer with the preferable valve orientation and desired dimension was achieved.

CHAPTER 4

THE EFFECT OF SINTERING PROCESS ON THE DIATOM MONOLAYER DEPOSITED ON SILICON SUBSTRATE: BONDIND OF THE DIATOM ON THE SUBSTRATE

4.1 Introduction

Bonding diatoms on a substrate is one of the crucial factors which enables using the diatoms for potential applications. However, only a few research groups were focusing on bonding SiO_2 or, Si diatoms onto a substrate. Losic et al.[28] bonded diatom frustules with a poly-l-lysine (PLL) treated Si substrate. The bond strength was not investigated and the bonding between PLL and the diatoms might merely rely on weak electrostatic interaction. Moreover, it was found in a preliminary experiment as part of this thesis that the PLL-treated glass substrate disrupted the monolayer formation. Chandrasekaran et al. modified the surface of Si-diatom with organic thiols via hydrosilylation before attaching the thiol-modified Si-diatoms on Au-coated glass slides with the goal of fabricating a photocathode for water splitting[23]. Sulfur compounds are weakly bound (physisorbed) to the Au(0) surface. [29]. The Au-S bonds are partially electrostatic (more that 65% electrostatic) and partially covalent (less than 35% covalent) [41]. Moreover, using molecular linkage between the diatoms and the substrate creates an interfacial layer which may form an insulating layer that contributes to electron scattering in electronic devices. Thus, directly bonding diatom frustules on a substrate without any molecular linkage will ensure the unimpeded transport of electrons from the diatom frustule through the substrate.

Pan et al. directly bonded SiO_2 diatoms on a Si substrate at 75 °C, assisted by hydrofluoric acid (HF) and applied pressure [8]. The diatoms were bonded to the substrate via Si-O-Si bonding as shown in Fig. 4-1. Other than the fact that heating HF would create harmful vapor or the pressure would crush the diatom structure, this bonding process cannot be used to bond Si diatoms on a substrate. Even if one wants to convert the bonded SiO_2 diatoms from this bonding process into Si diatoms using magnesiothermic conversion, the Si-O-Si bonds would be destroyed during the conversion process.

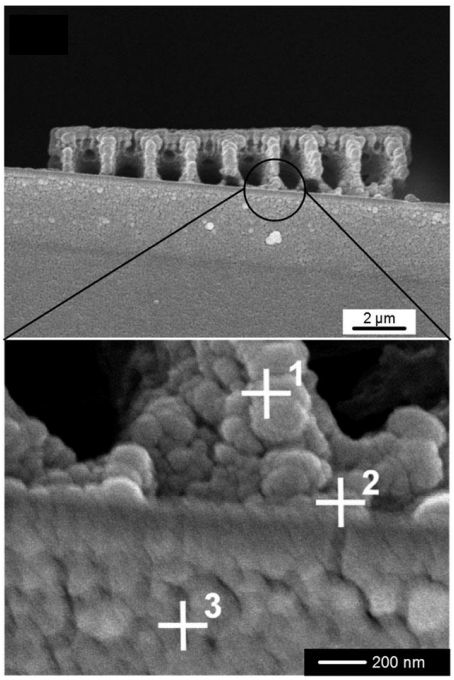

Figure 4-1 Cross-section images of the bonded diatom using HF and pressure. The top image shows that the diatom was bonded to the substrate so well that it became one with the substrate. The bottom image reveals the interface between the diatom and the substrate. Area 1 is the diatom (34.02% Si and 65.98% O). Area 2 is the interface region (61.98% Si and 38.02% O). Area 3 is the silicon substrate (99.71% Si and 0.29% O)[8].

Although the sintering process at high temperature has been used to bond silica nanoparticles on a Si wafer substrate[30], [31], this process has not been used to bond SiO_2

diatoms and a Si wafer due to the concern of the high temperature potentially destroying the diatom nanostructure[8] . However, there are no reports about the highest temperature that the diatom structure can tolerate. Therefore, in this thesis, the direct bonding of SiO_2 diatom (*C.wailesii*) on a Si wafer was investigated, using a high temperature sintering process. The SiO_2 diatoms were closely-packed as a monolayer on the substrate before the sintering process to maximize the contact area between each diatom and the substrate.

4.2 Materials and Method

4.2.1 Sintering process

In a $MoSi_2$ furnace (Deltech), a closely-packed diatom monolayer, deposited on a silicon wafer, was placed on an Al_2O_3 rectangular plate to prevent contamination from a sample holder (Al_2O_3 circular plate), and then covered with a pericline lid to prevent contamination from furnace elements. The sample was heated at 2°C/min to the target temperature (1000°C, 1100°C, 1125°C, 1150°C, or 1200°C), holding for 2 hours before it was cooled down to room temperature at a rate of 1.5°C/min. After the sintering, the un-bonded diatoms were gently washed away with deionized water and dried by N_2 flow. SEM images were obtained using an XL30 environmental scanning electron microscope (ESEM) FEG and a Phenom World Environmental SEM. Energy dispersive X-ray (EDX) analysis was obtained using the XL30 ESRM FEG.

4.2.2 Bond strength measurement

Before bond strength measurement, a tungsten wire (0.15mm in diameter) was calibrated using an added-mass method adapted from Lamoureux et al.[42] To observe the vertical deflection of the wire, a dissecting microscope with a measuring reticle was tilted 90°on to its side using an universal boom stand. The wire was fixed on a micromanipulator so that it was perpendicular to the optical axis of the microscope. Small stainless-steel rings with a known mass were attached to the tip of the wire, while the vertical deflection of the wire was recorded. The spring constant was calculated from the deflection (in mm) divided by weight (in N).

Under an optical microscope, the wire was used to push sintered/bonded valves using the micromanipulator. In order to obtain the deflection of the wire, micrographs were recorded using a Video camera (Canon 80D DSLR) attached to the optical microscope and analyzed using VirtualDub 1.10.4 and ImageJ. The bond strength is deflection time the spring constant of the wire.

4.3 Result and Discussion

4.3.1 Bonding/Sintering Process

The diatom monolayers on silicon wafers were heated at various temperatures, 1000°C, 1100°C, 1125°C, 1150°C, and 1200°C, for two hours under ambient atmosphere. After the high temperature treatment, the bonded diatoms on the silicon wafers were washed with deionized water and blown dry with nitrogen gas to remove unbound diatoms. The optical micrographs of the sintered diatom monolayer before and after the washing

process are shown in Fig. 4-2. The percentage of the diatoms remaining on the wafer after the washing process is demonstrated as a plot in Fig. 4-3. It shows that when the temperature was increased, more valves were bonded to the silicon wafer.

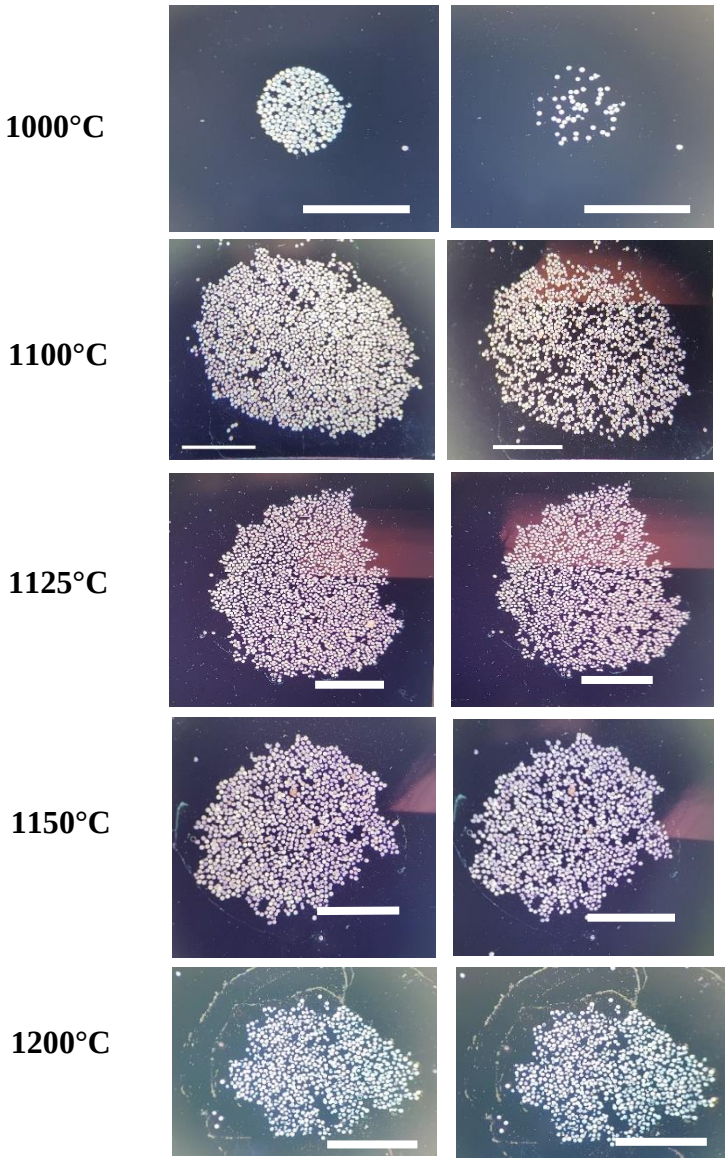

Figure 4-2 The photographs of the sintered diatom monolayers on silicon substrates before (left row) and after (right row) the washing process. The color of the silicon substrates is due to the thermally grown oxide layer during the sintering process.

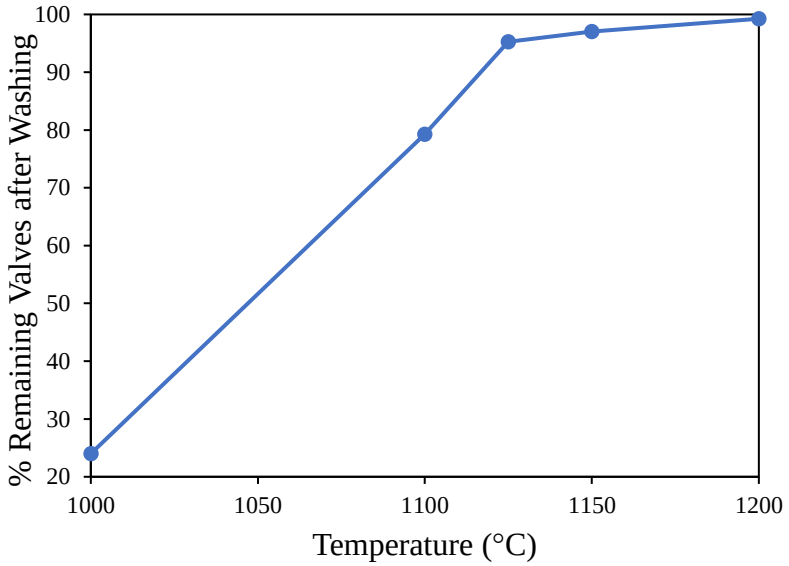

Figure 4-3 A plot demonstrating the percentage of valves that remained on the substrate after heating at various temperatures, followed by the washing process. The number of the valves on the substrate was counted using the Gwyddion program.

The SEM images of sintered diatoms on the substrate are shown in Fig. 4-4 to Fig. 4-8. The SEM images (Fig. 4-4a, Fig. 4-5e, Fig. 4-6k, Fig. 4-7q, and Fig. 4-8w) reveal that the orientation of the valves is mostly convex-down (external surface was in contact with the substrate), enhancing the chance for the diatoms to be bonded to the surface. Moreover, it shows the change of the micro-nano structure of the valves at the different temperatures. The structure tends to adhere more to the substrate at higher temperature. At 1000°C with only 24% of the remaining diatoms, the adhesion was not obvious and the diatom valves look intact (Fig. 4-4b and Fig. 4-4c). At 1100°C, neck formation (the onset of sintering process occurred when surface atoms of silica diffuse to the substrate) was observed at the interface between a valve and the substrate (Fig. 4-5j) since this temperature is the point where surface diffusion in silica nanoparticles was activated[30]. This neck formation was

not observed at 1000°C (Fig. 4-5d), but appeared at 1100°C and above (1125°C (Fig. 4-6p) and 1150°C (Fig. 4-6v)).

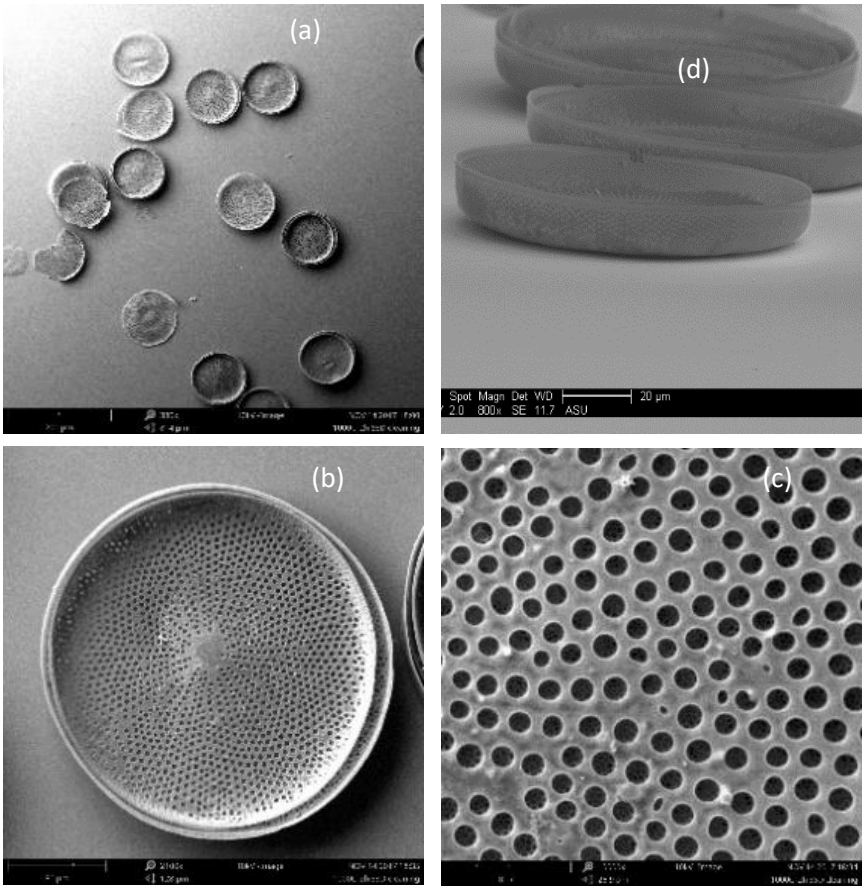

Figure 4-4 SEM images of sintered diatoms at 1000°C. The valves were well preserved (a-c) without neck formation observed (d).

At 1100°C, with 79% of the valves remaining after washing, some valves obviously sintered into the substrate, indicated by the darker region of some internal valves (Fig. 4-5f). Fig. 4-5g shows the details of the adhesion region from the internal valves with preserved nano- micro pores. Moreover, the intricate nanostructure of cribrum on the external valves was still preserved at such high temperature, though some of the cribellum disappeared (Fig. 4-5h-i).

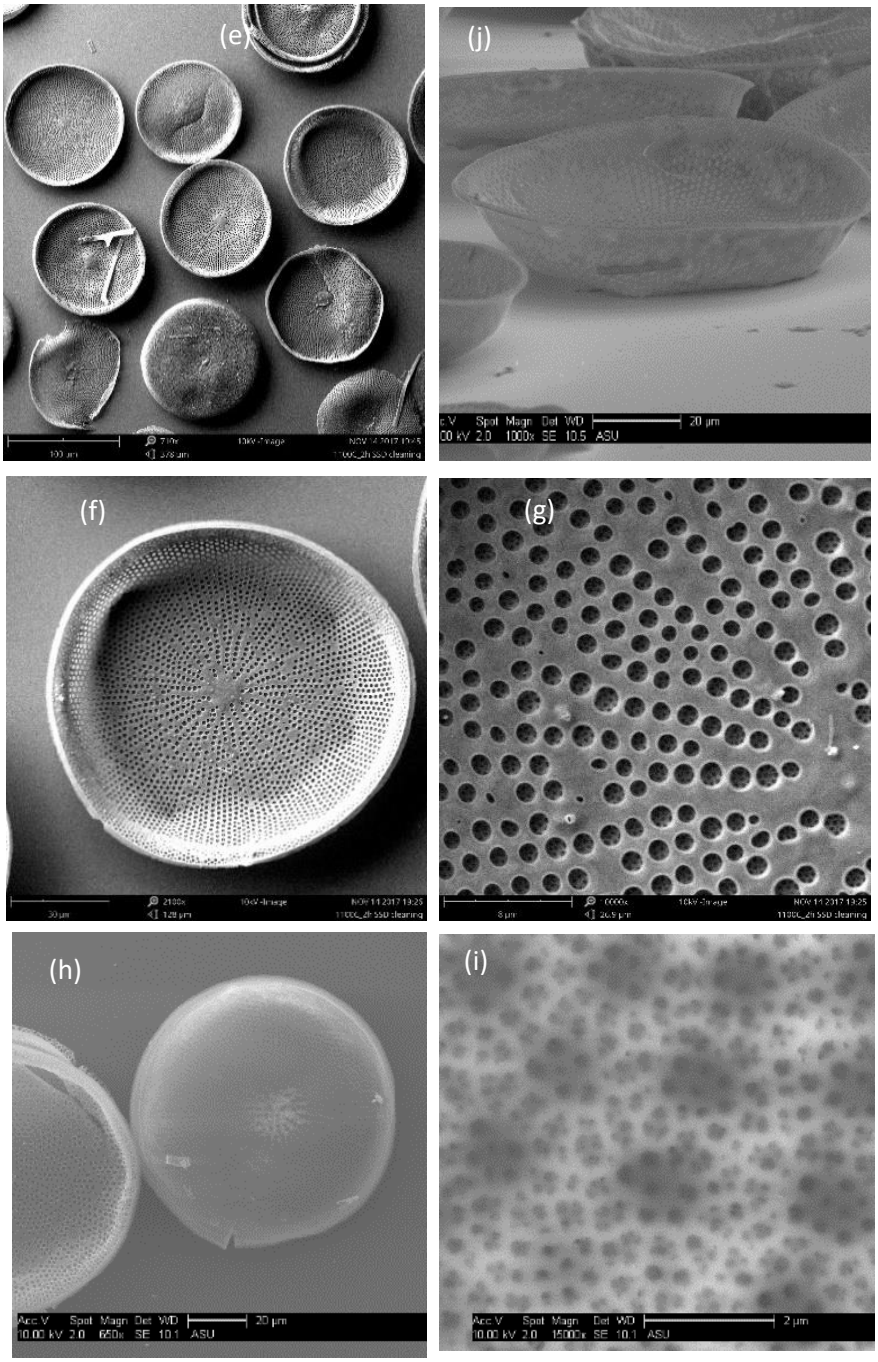

Figure 4-5 SEM images of sintered diatoms at 1100°C. The sintering started at 1100°C (e-j). The darker region of a valve shows evidence of sintering (f) with preserved-nano pores inside (g). The intricate nanostructure on the external valve was observed, though some of the cribellum started to disappear (h,i). The neck formation starts to occur at this temperature (j).

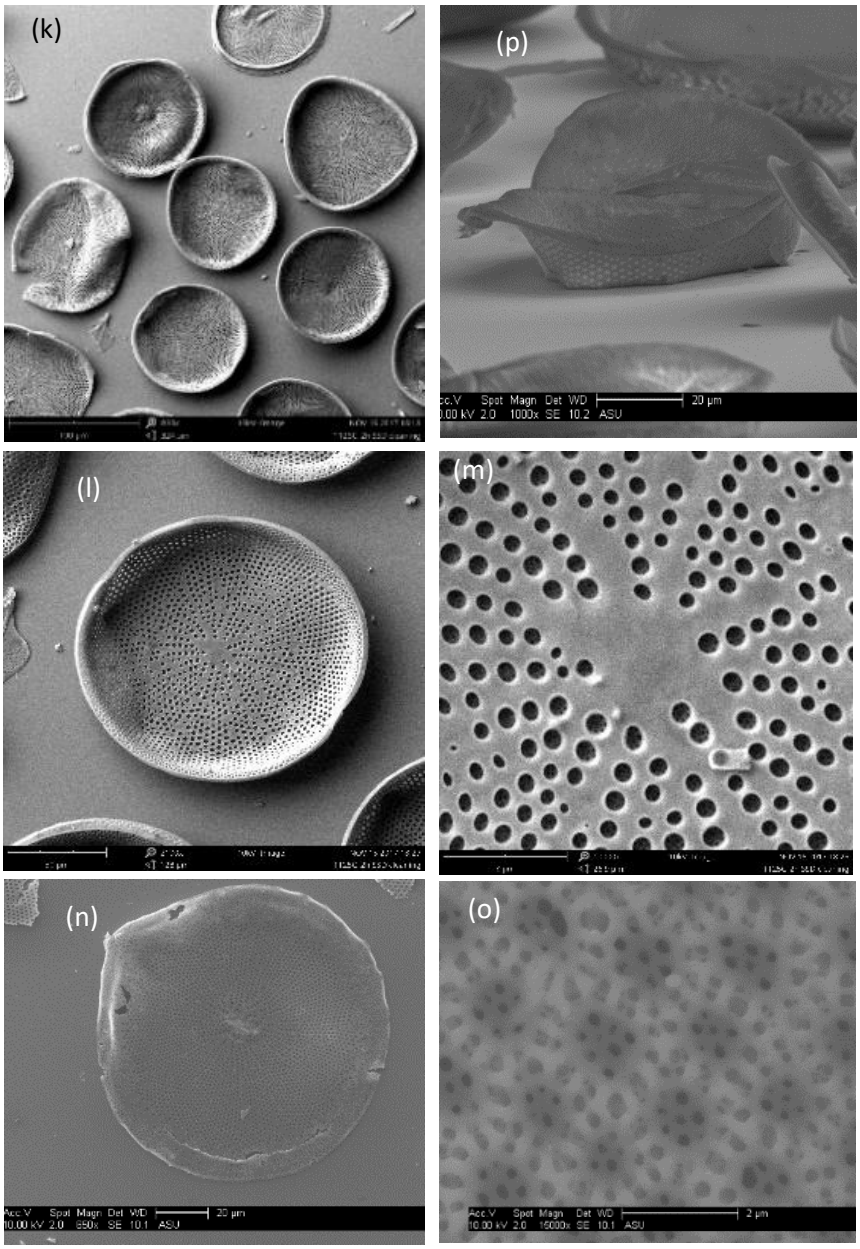

Figure 4-6 SEM images of sintered diatoms at 1125°C. The neck formation can be seen in (p). At this temperature, more sintered valves were observed (k) and more of the cribellum structure disappeared (n, o). The shrinkage of nano-micro pores can be observed (l, m)

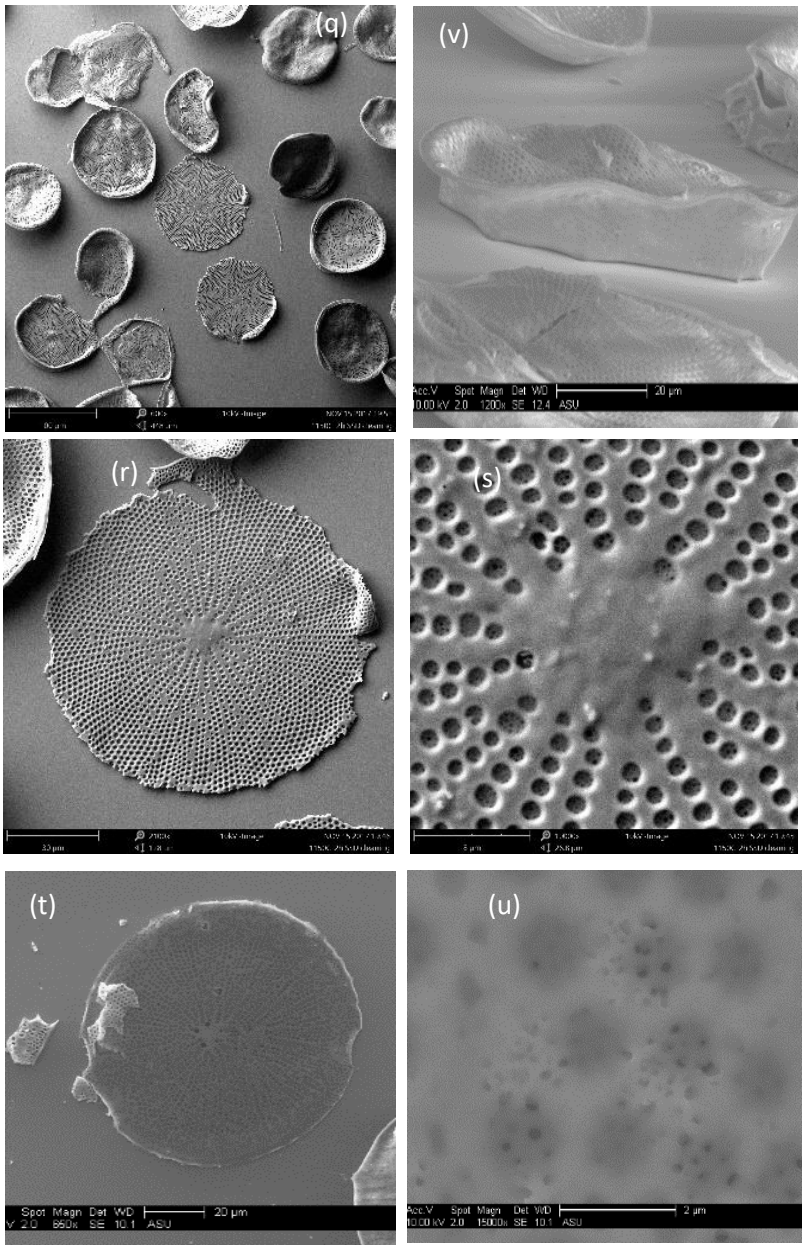

Figure 4-7 SEM images of sintered diatoms at 1150°C. The neck formation can be seen in (v). The valves became more wrinkled (q) and the pores of cribrum and cribellum disappeared (t, u). The shrinkage in nano-micro pores was observed (r, s).

At 1125°C, it's more obvious that the valves adhere to the surface as more internal valves with dark regions were found in this condition (Fig. 4-6k). The adhesion areas still

show the nanopores inside the micropores (Fig. 4-6l and Fig. 4-6m), though shrinkage of the nanopores is observed. On the external valve surface, the cribrum was preserved but more of the cribellum structure was destroyed (Fig. 4-6n and Fig.4-6o).

At 1150°C, the valves start to lose the circular shape and become wrinkled (Fig. 4-7q). From the internal valve's view, the nano- and periodic micro-pores can be observed (Fig. 4-7r and Fig. 4-7s). However, some valves show shrinkage in nano-pores. On the external valve surface, pores of cribrum started to disappear while the cribellum was almost completely destroyed (Fig. 4-7t and 4-7u).

At 1200°C, the valves started to melt and the nano-micro structures in both external (Fig. 4-8y and Fig. 4-8z) and internal valves (Fig. 4-8w and Fig. 4-8x) disappeared. It is also observed that, at higher temperature, some valves lost their vertical component, as shown in the case of the 1150°C condition (Fig. 4-7r), and particularly in the case of the 1200°C condition (Fig. 4-8w). In addition, when the valves lost their vertical component, their horizontal component seemed to completely adhere to the substrate (Fig. 4-7r).

4.3.2 Interface Investigation

To study the interface between the valves and the substrate, samples that were sintered at 1125°C, 1500°C, and 1200°C were cleaved in order to examine the cross-section area. The cross-section images reveal that the valves fused into the thermally grown oxide (TGO) layer on the silicon wafer. At these temperatures, the diatoms were firmly sintered into the substrate (Fig. 4-9 to Fig. 4-11). The cross section of the sample processed at

1125°C shows that while fusing with the substrate, the nano-micro pores of the valves are still preserved (Fig. 4-9).

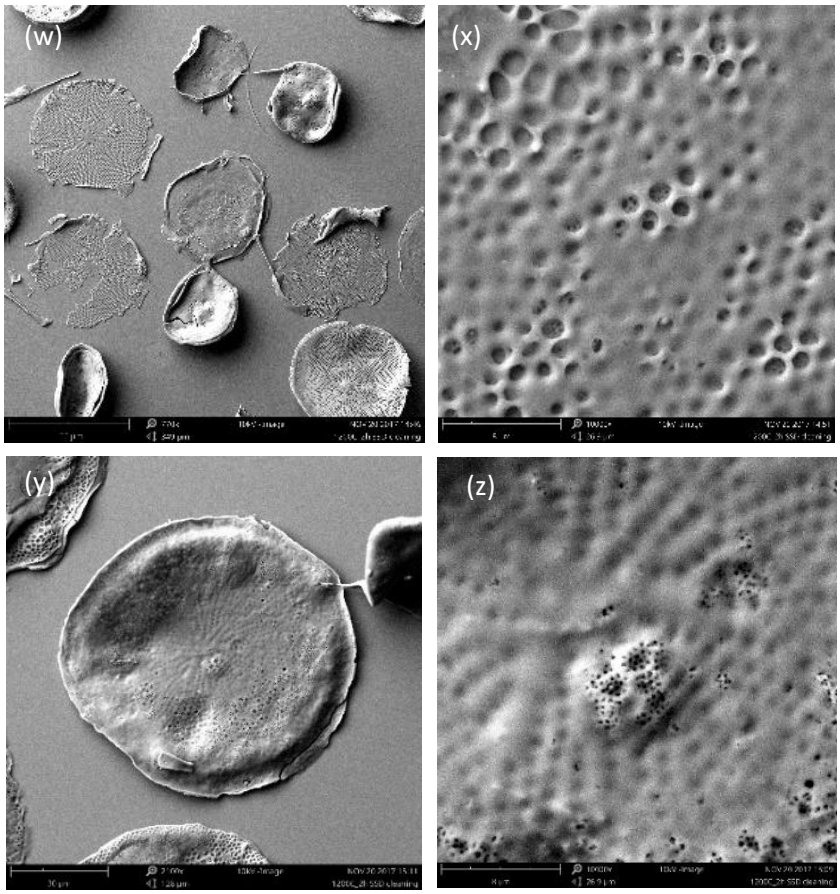

Figure 4-8 SEM images of sintered diatoms at 1200°C. The valves started to melt and the nano-micro structures were destroyed.

When the temperature was increased to 1150°C, a larger area of the valves fused into the substrate compared to those processed at 1125°C.. The nano-micro pores are preserved in some valves (Fig. 4-10h and Fig. 4-10i), but in some valves the nano-pores disappeared (Fig. 4-10g). At 1200°C, although the valves completely merged with the substrate (Fig. 4-11j), the nano-micro pores are destroyed (Fig. 4-11k). Most importantly,

the chamber-like structure of areola is still observed at 1125°C (Fig. 4-9e) and 1150°C (Fig. 4-10g and Fig. 4-10i) while it is destroyed by the high temperature treatment at 1200°C (Fig. 4-11k). The deformation and shrinkage in the valves observable on the cross-section images agrees with the top view images in Fig. 4-6 to Fig. 4-8.

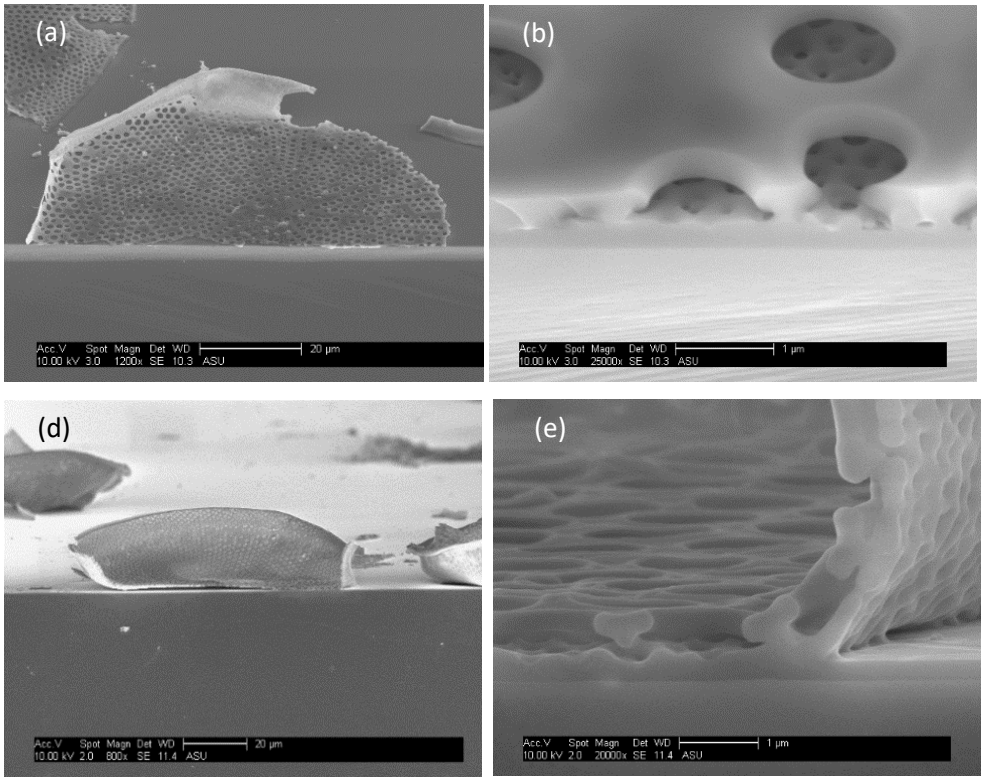

Figure 4-9 SEM cross-section images of sintered diatom at 1125°C. The areolae are observed in this condition.

At high temperatures (1125°C and higher), volume diffusion, which is responsible for the transport of matter from the bulk (the diatom valves) to the neck region, is activated. Such high temperatures also activate diffusion along the valve-substrate interface. The driving force for these diffusion mechanisms is associated with the minimization of the free surface energy, which is being achieved by reducing the surface area[30]. Thus, these

diffusion mechanisms may be associated with the shrinkage in nano-micro pores of the valves found at these high temperatures.

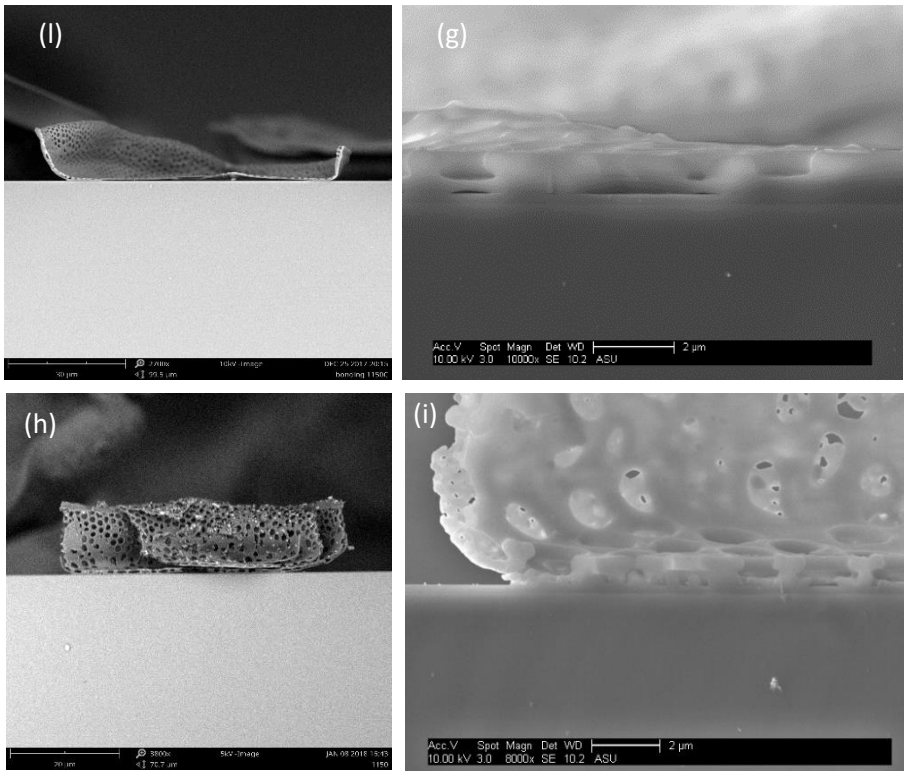

Figure 4-10 SEM cross-section images of sintered diatom at 1150°C. The contamination of a small particle can prevent the sintering process (l). A larger external surface area of the valves sintered into the substrate. The areolae are observed in this condition.

In addition, the roughness of the external surface of valves did not impact the bonding process as much as contamination of small particles. As shown in Fig. 4-10l, the two ends of a valve surface could sinter into the substrate, but the entire valve could not bond to the surface because there was a particle underneath the valve. Thus, it is highly important to control the particles in diatom samples as much as possible.

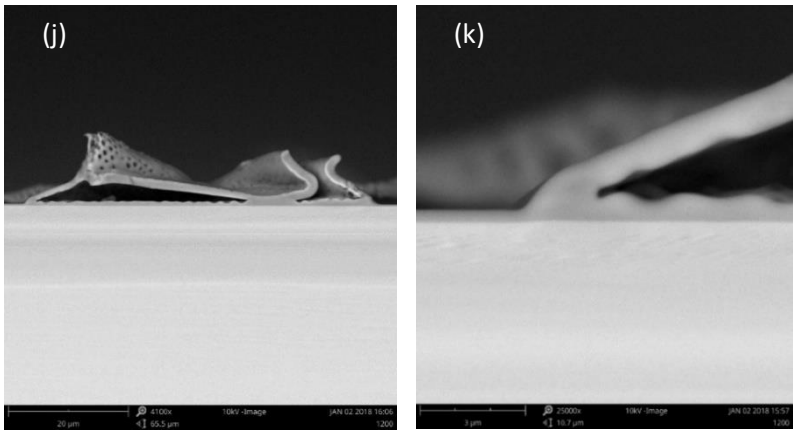

Figure 4-11 SEM cross-section images of sintered diatom at 1200°C. The high temperature, particularly at 1200°C, also destroyed the nano-micro structures. The areola is not observed in this condition.

Elemental components at the interface between the valves and the substrate were investigated using EDX which revealed oxygen and silicon contents in a sample processed at 1150°C (Fig. 4-12 and Table1). The atomic ratio of Si to O in the bulk material (area 1) is around 0.5, indicating the presence of silica in the diatom. At the interface region (area 2-4), the oxygen content was less than that in the bulk diatom at 50%. The TGO layer without bonded a valve (area 6) had half of the oxygen content compared to the interface.

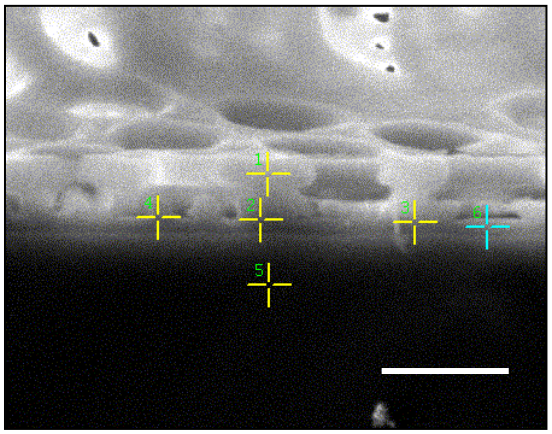

Figure 4-12 Cross-section of sintered diatoms on a silicon wafer at 1150°C with marked areas for EDX (The scale bar is 2μm.)

Table 4-1: Atomic percentage of elements in the cross-section areas in Fig. 4-12

Area	Elements (%Atom)	
	OK	SiK
1	65.69	34.31
2	32.98	67.02
3	28.42	71.58
4	28.05	71.95
5	00.71	99.29
6	12.84	87.16

EDX indicates that the element content at the interface is not from the TGO layer, but is associated with the bonding between the valve and the substrate. Since necking formation and other diffusion mechanisms can be activated at these temperatures, it is possible that the diffusion is not only responsible for the shrinkage but also the bonding between the diatoms and the substrate.

4.3.3 Bond Strength

The bond strength of the diatoms on a silicon wafer was measured using the shear force that was necessary to remove a bonded valve. The shear force was applied via a tungsten wire. The shear force was measured as the spring constant (0.055N/m) of the tungsten wire times the deflection of the wire. The bond strength was then calculated as the shear force per valve.

In the bond strength measurement, the valves processed at 1000°C easily detached from the substrate without any wire deflection to be observed. Thus, it was assumed that the bond strength was weak. The bond strength as a function of sintering temperature

(1100°C, 1125°C, 1150°C) is demonstrated in Fig. 4-13. The figure shows that at higher temperature, the bond between the valves and the substrate is stronger. Moreover, for the sample processed at 1200°C, valves, which were flattened by the high temperaturetreatment, were broken by the sheear force This made it harder to calculate the bond strength as the deflection of the wire was caused not only by the bond, but also the strength of the valves themselves. This indicates that the bond between the valves and the substrate is so strong that the valves broke before they were removed from the substrate by the wire. The bond strength measurement agrees with the percentage of remaining valves (Fig.4-3).

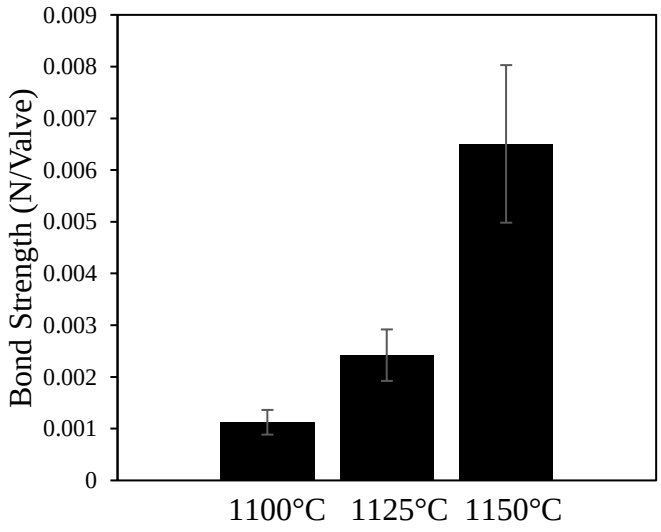

Figure 4-13 The bond strength vs temperature plot. The bond strength was higher when the temperature increased. The error bars were calculated from standard variation of each sample.

4.4 Conclusion

The percentage of diatom valves which sintered into the Si substrates increased with increasing temperature. The valves started to sinter into the substrate at 1100°C, indicated by the neck formation first observed at this temperature. The sintering process was found to cause shrinkage in nano-micro pores and destroyed the nano-micro structure of the diatoms at a particular temperature. The nanostructures are more sensitive to the high temperature treatment than the microstrucures. The cribellum, the most intricate nanostructure of the diatom, is observed at 1100°C, but started to disappear at 1125°C. The cribrum is still observed at 1125°C, but disappeared at 1150°C. The valve melted and completely fused with the substrate at 1200°C. The chamber-like structure of areola (microstructure) tolerates the high temperature treatment up to 1150°C. The nano-micro structure of the diatom disappeared at 1200°C. The bond strength measurement revealed that the bond strength between the valves and the substrate is directly proportional to the processing temperature.

CHAPTER 5

SILICON SINTERED DIATOM MONOLAYER AND ITS OPTICAL PROPERTIES

5.1 Introduction

Since Si-nanostructures are used for solar energy conversion[16], [17] and energy storage[11], [18], converting SiO_2 diatoms into Si with preserved nanostructures may allow us to use the diatom frustules for those applications. The pioneering diatom conversion work reported by Bao et al.[19] who used magnesium vapor from magnesium metal to convert silica diatoms at high temperature using the following chemical reaction:

$$2Mg(g) + SiO_2(s) \rightarrow 2MgO(s)/Si(s) \quad (5.1)$$

MgO was then selectively dissolved by 1M HCl. The Si diatoms were photoluminescent, and they proposed that the converted diatoms were possibly used in microscale gas sensing. Though the converted nanostructures of the Si diatoms were well preserved, the vapor pressure from magnesium metal was high enough to drive the formation of magnesium silicide, Mg_2Si [20], described by the following reaction[43]:

$$SiO_2(s) + 4Mg(g) \rightarrow 2MgO(s)/Mg_2Si(s) \quad (5.2)$$

Luo et al. performed a similar experiment but added NaCl as a heat scavenger. they found that SiO_2 diatoms were converted into Si-diatoms without the formation of Mg_2Si [21]. However, addition of NaCl may introduce mobile Na^+ ions into Si-diatoms, decreasing the Si performance for photovoltaic applications.

Furthermore, to avoid the formation of magnesium silicide, Chandrasekaran et al.[22] decreased the molar ratio of Mg: SiO_2 to 1.25:1. They reported that the diatoms were successfully converted into silicon with a preserved structure. Boron-doped Si-diatoms were then used to fabricate a photocathode which was able to produce hydrogen via photoelectrochemical reaction [23]. However, based on this approach, some diatoms did not react with magnesium since the magnesium amount was not equivalent to the silica amount as shown in equation 5.1. The incomplete reaction based on this particular molar ratio of Mg and SiO_2 was verified in a preliminary experiment as part of this thesis. The preliminary experiment revealed that when Mg and diatoms were mixed thoroughly, Mg_2Si was formed as one of the products (Fig. 5-1a, red spectrum). When the reactants were separated (not thoroughly mixed), Si was formed without Mg_2Si (Fig. 5-1a, blue spectrum). Yet, some unreacted diatoms (white color) accompanied the Si product (gold color) as shown in Fig. 5-1b.

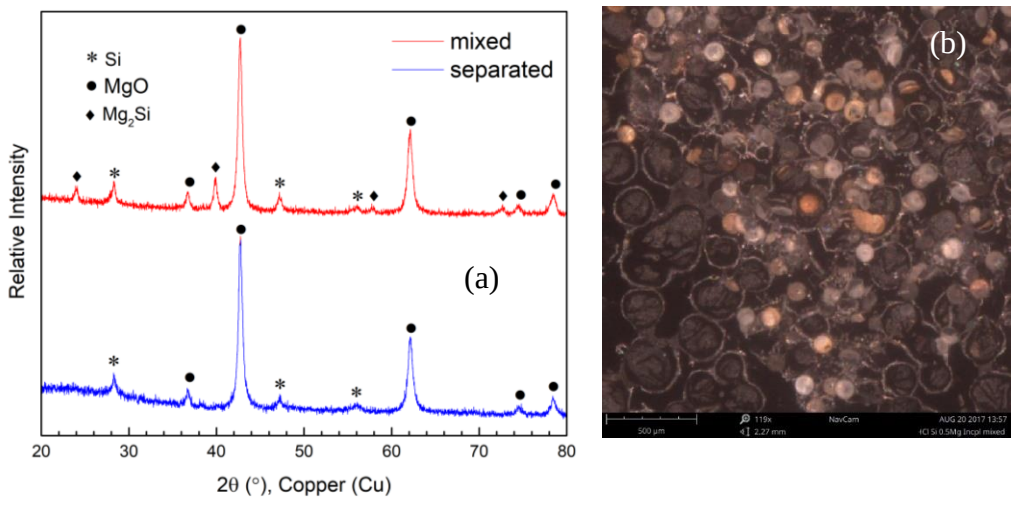

Figure 5-1 X-ray diffraction (XRD) spectra from the magnesiothermic conversion using the molar ratio of Mg:SiO_2 as 1.25:1 (a). A mixture of Si, MgO, and Mg_2Si was obtained when the reactants were thoroughly mixed (red spectrum). The undesired Mg_2Si was not observed when the two reactants were separated (blue spectrum). This route,

however, could not convert all diatoms into Si. The unreacted diatoms (white) were remained with the Si diatoms (gold). The reference codes of the spectra are 00-004-0829 for MgO, 00-005-0565 for Si, and 00-035-0773 for Mg_2Si. The details of the reactor used to perform the conversion can be found in section 5.2.

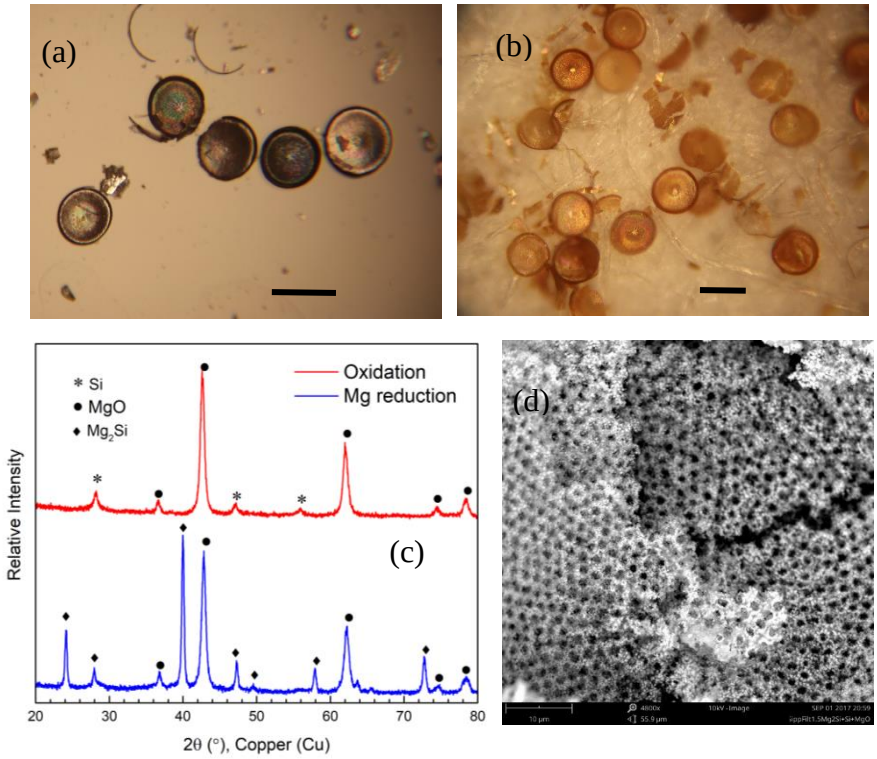

Figure 5-2 Preliminary results from the two-step conversion process. The black Mg_2Si diatoms were obtained after the reduction with excess Mg (a) and the gold Si diatoms were obtained after the subsequent oxidation (b). The scale bar is 100 μm. The XRD spectra in (c) confirm the presence of Mg_2Si from the reduction and Si from the oxidation. The SEM image in (d) shows the collapsed Si diatom after MgO selective dissolution. The reference codes for the spectra are 00-004-0829 for MgO, 00-005-0565 for Si, and 00-035-0773 for Mg_2Si. The details of the reactor can be found in 5.2.

In 2016, Liang et al. suggested another path for the conversion. They completely converted SiO_2 diatoms into Mg_2Si/MgO diatoms using excess Mg vapor, then converted the Mg_2Si into Si/MgO composite via an oxidation reaction[24]. This two-step conversion is appealing because, in theory, it can turn all Mg_2Si into Si diatom without leaving

unreacted diatoms. A preliminary experiment using this method was carried out as part of this thesis. Fig. 5-2 demonstrates that after the reduction, black Mg_2Si diatoms (Fig. 5-2a) and after the oxidation gold Si-diatoms (Fig. 5-2b) were obtained. The XRD spectra (Fig. 5-2c) show the Mg_2Si/MgO product after the reduction (blue spectrum) and the Si/MgO product after the oxidation. However, after the MgO selective-dissolution in 1M Hydrochloric Acid, the diatom structure collapsed as shown in Fig. 5-2d. The reason for the collapse is based on the molar volume of Mg_2Si/MgO being significantly higher than that of SiO_2 or Si/MgO [25]. This causes the diatom structure to expand after the reduction, then collapse after the oxidation and MgO-selective dissolution.

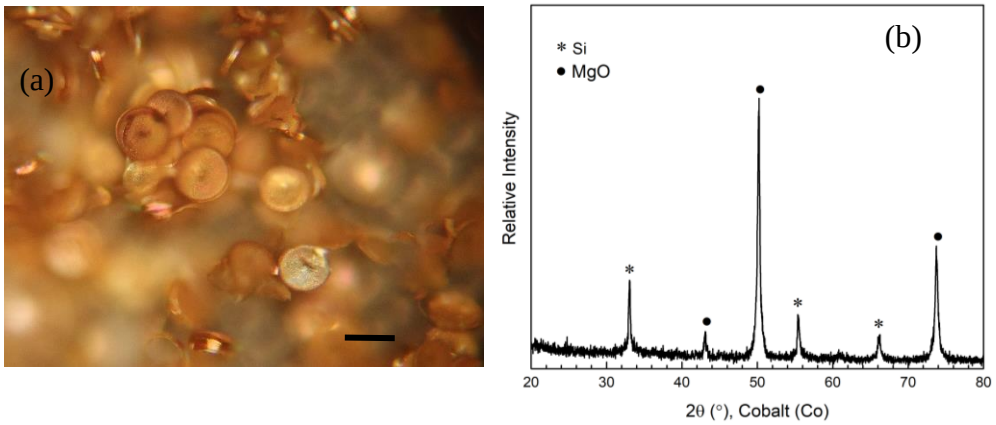

Figure 5-3 The photograph of gold Si diatoms obtained after magnesiothermic conversion using Mg_2Si as Mg vapor source (a) and the corresponding XRD spectrum (b). The scale bar is 100 μm. The reference codes of the spectra are 00-004-0829 for MgO and 00-005-0565 for Si. The details of the reactor can be found in 5.2.

To completely convert SiO_2 into Si diatoms with well-preserved structure, Gordin used Mg_2Si as the Mg vapor source instead of using magnesium metal [26]. With the lower Mg vapor pressure, SiO_2 diatoms were converted directly into Si without Mg_2Si formation. Moreover, the molar volume of MgO/Si is slightly different that SiO_2, thus preventing the

diatom structure from collapsing [26]. This process was proven to be effective according to the experiments carried out as part of this thesis. The XRD spectrum of the obtained Si/MgO diatoms obtained using this process (Fig. 5-3a) is shown in Fig. 5-3b.

Therefore, this magnesiothermic conversion has been used for the conversion of the sintered SiO_2 diatom on the silicon substrate into silicon. This conversion enabled the Si-diatom on the substrate to be spin-coated with Poly(3,4-ethylenedioxythiophene): polystyrenesulfonate (PEDOT: PSS), a highly conductive polymer with relatively high work function[32], to provide a hole-collection layer in a photovoltaic device. The optical and electrical properties of PEDOT:PSS coated Si-diatom on the substrate could then be investigated using reflectance spectrometry and photoresponse measurements.

5.2 Materials and Method

5.2.1 Magnesiothermic conversion

A metal-seal (Cajon VCR)stainless steel reactor (0.5 inches inner diameter) with stainless-steel gaskets (Swagelok Southwest, USA) was used in this work. This reactor was also used for the preliminary experiments.

For the one step conversion adapted from Chandrasekaran et al.[22], the powder dried diatoms and Mg shards with 0.5g-Mg: 1g-SiO_2 were loaded into the VCR-reactor (Fig. 5-4), which was closed in a glovebox with Ar atmosphere. The two reactants were mixed and separated (about 1 cm in distance) to examine the effect of the mixture on the reaction. A Muffle furnace was heated to 650 °C before the reactor was inserted in the furnace and held at this temperature for 2.5 hours.

For the two-step conversion adapted from Liang et al.[24], the powder dried diatoms and Mg shards with 1.5g-Mg: 1g-SiO_2 were loaded into the VCR-reactor, which was closed in the glovebox. The two reactants were separated about 1 cm in distance. The Muffle furnace was heated to 650 °C before the reactor was inserted in the furnace and held at this temperature for 2.5 hours. The reacted diatoms (Mg_2Si- black diatoms) were oxidized in air in the Muffle furnace at 600 °C for 5 hours.

For the decreased Mg-vapor pressure method adapted from Gordin[26], the powder diatoms (0.0584 g) and Mg_2Si (0.2 g) were loaded into the VCR-reactor, which was closed in the glovebox. The two reactants were separated about 1 cm in distance. The reactor was placed in the Muffle furnace and heated at 5 °C/min. to 750 °C. The reaction was held at this temperature for 2 hours before cooling down to room temperature in the furnace.

After the preliminary experiments, the most effective method was used to convert the sintered SiO_2 diatom on the substrate into silicon. A sintered-sample (with or without diatoms) was inserted in the VCR-stainless steel reactor and located at one end of the reactor while 0.2g-Mg_2Si (Sigma Aldrich) was homogeneously spread on the other end. VCR-stainless steel face seal fitting (gaskets and caps) were used to seal the reactor. Mg_2Si was used as the Mg vapor source[26]. The Mg_2Si loading and reactor sealing were done in a glovebox under Ar atmosphere in order to fill the reactor with inert gas. In a Muffle furnace (Thermolyne) with air atmosphere, the tightly sealed-reactor was heated at 5°C/min to 750°C holding for 2hrs before cooling down to room temperature in the furnace. The reacted sintered diatom on a wafer was then immersed in 1M HCl solution (Fisher

Scientific, USA) for 30 min to selectively dissolve MgO, followed by the removal of surface-grown SiO_2 using 5% aqueous HF[21].

Figure 5-4 The image showing VCR-stainless steel reactor.

SEM images and EDX spectra were obtained using the XL30 ESEM. XRD spectra were recorded on a Powder X-ray Diffractometer (Siemens Bruker-D5000). Fourier-Transform Infrared Spectra (FTIR) were investigated using a Thermo-Nicolet Magna-IR 560 spectrometer in transmission mode. The reflection spectra of the samples were investigated using a Perkin Elmer spectrometer (Lambda 950S).

5.2.2 PEDOT:PSS coating

The PEDOT:PSS solution with 5 (v:v)% dimethyl sulfoxide, 1 (v:v)% Triton X-100, and 0.3 (v:v)% 3-glycidoxypropyltrimethoxysilane (GOPS)[32] was spin-coated on Si wafers at 500 rotations per minute (rpm) for 5 s followed by 3500 rpm for 60 s[44]. The spin-coated films were heated at 140°C for 30 min using a hot plate in ambient air in order

to enable the cross-linking process between PEDOT:PSS and GOPS[45]. Ga:In eutectic was applied to the back of the wafers to form an ohmic contact. The samples were immediately mounted onto a Cu supporting plate. Epoxy or PMMA glue was applied to each edge of a wafer to seal the wafer to the support.

5.2.3 Photocurrent Measurement

The photocurrent was investigated using a Xe-lamp (75W) as the light source, passing through a single grating monochromator (Jobin-Yvon 320, 1200 lines/mm) as a wavelength filter. The samples were measured on a probe station with 2mm Ø fiber optic illumination. The back contact of a sample was connected to ground while the front contact was connected to an SR570 current preamplifier to convert photocurrent (I_{SC}) into voltage. The voltage equivalent from the SR570 current preamplifier and reference signal from a chopper wheel were sent to a SR830 Lock-In amplifier. LabView was used to scan the incident wavelength and record the lock-in output and plot the spectral response in the form of photocurrent versus wavelength. The obtained photocurrent was normalized against the light intensity recorded with a standard Si-photodiode (Thor labs).

5.3 Results and discussion

5.3.1 Magnesiothermic conversion

Diatoms sintered on the substrate at 1125°C were used in the magnesiothermic conversion, because these sintered diatoms exhibited sufficient bonding while the cribrum and foramen pores of the valves were preserved. The reduction was followed by MgO-

selective dissolution using 1M HCl solution and residual SiO_2 removal using HF. The converted diatoms have a goldish-brown color.

The crystalline structure of the converted diatoms was investigated by XRD (Fig. 5-5). The XRD patterns indicate the presence of MgO (reference code 00-004-0829) and Si (reference code 00-005-0565) after the conversion, while Mg_2Si crystals were not observed (Fig. 5-5a). MgO was selectively dissolved from the Si sample by immersing the sample in 1M HCl for 30min (Fig. 5-5b). The XRD analysis also reveals the presence of the (100) silicon wafer substrate at 82°(2θ) as shown in the insets. Thus, for the first time, the SiO_2 diatoms, which were sintered into a Si-wafer, were successfully converted into Si-diatoms.

The change in chemical bonds of diatoms on a wafer was tracked by FTIR spectroscopy as shown in Fig. 5-6. The sintered silica diatoms on the substrate show the infrared absorption line of Si-O-Si bonds at 1000 to 1300 cm^{-1} (stretching mode), 794 cm^{-1} (bending mode), and 464 cm^{-1} (rocking mode) (Fig. 5-6a). The infrared absorption at 616 to 619 cm^{-1} corresponds to Si-Si bonds in the silicon wafer used as the substrate. The absorption peaks related to Si-O-Si bonds disappeared after the selective dissolution of magnesium (before HF etching, Fig. 5-6b). Moreover, Fig. 5-6b shows infrared absorption at around 2100 cm^{-1} (stretching modes), 800 to 1000 cm^{-1} (bending mode), and 600 to 750 cm^{-1} (wagging modes), corresponding to $Si\text{-}H_n$ ($n\geq1$) bonds[46]. The absorption peak at around 1106 to 1107 cm^{-1} associates with oxygen interstitials in the silicon wafer[47]. The sample has similar infrared absorption after removing residual SiO_2 using HF (Fig. 5-6c).

The absence of Si-O-Si peaks and the presence of Si-H_n bonding before HF etching indicates that the amorphous silica was completely reduced in the magnesiothermic conversion process.

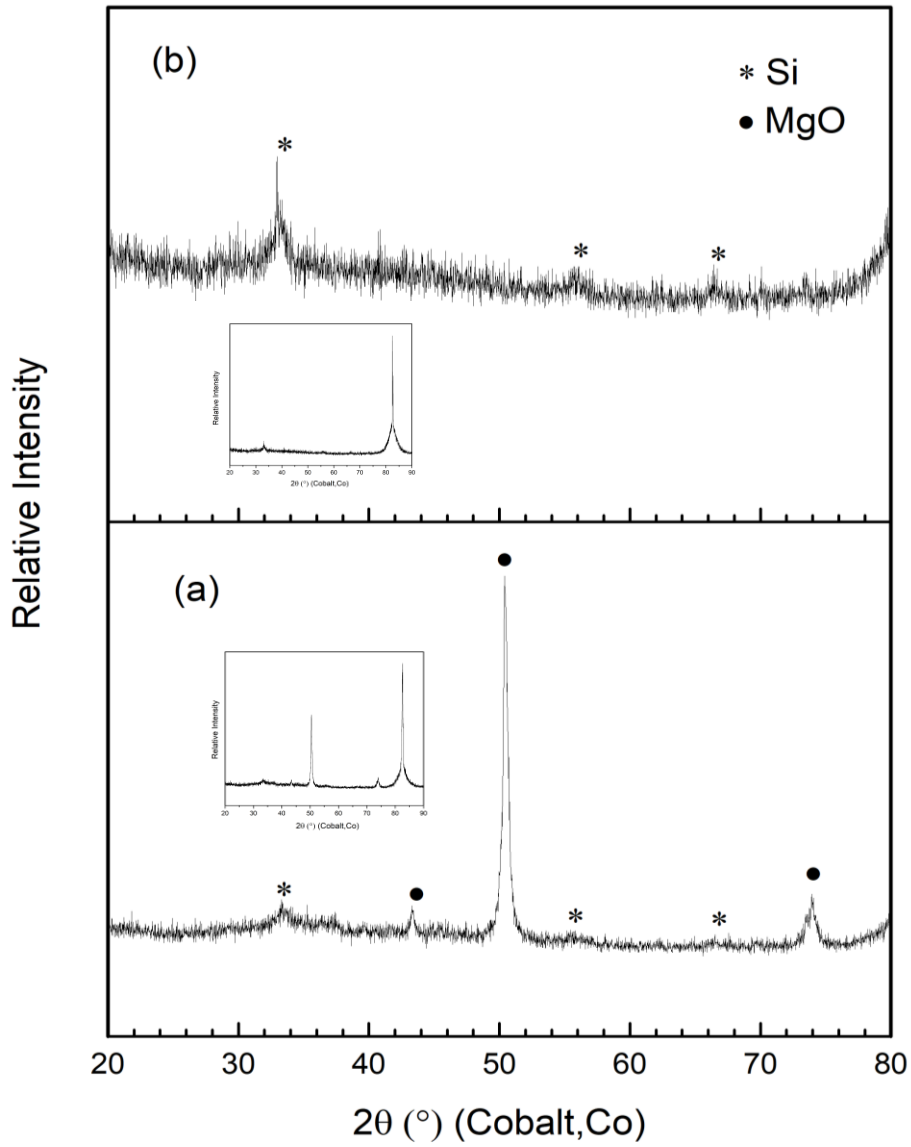

Figure 5-5 XRD spectra of the sintered diatoms on a Si-wafer substrate after the magnesiothermic conversion. (a) The XRD pattern reveals MgO and Si after the diatoms reacted with magnesium silicide at 750°C for 2 hours in VCR-stainless steel reactor filled with argon gas. (b) XRD pattern showing the Si-XRD pattern after MgO in (a) was selectively dissolved Si using 1M HCl solution. The insets show the presence of the (100) silicon wafer substrate at 82°(2θ).

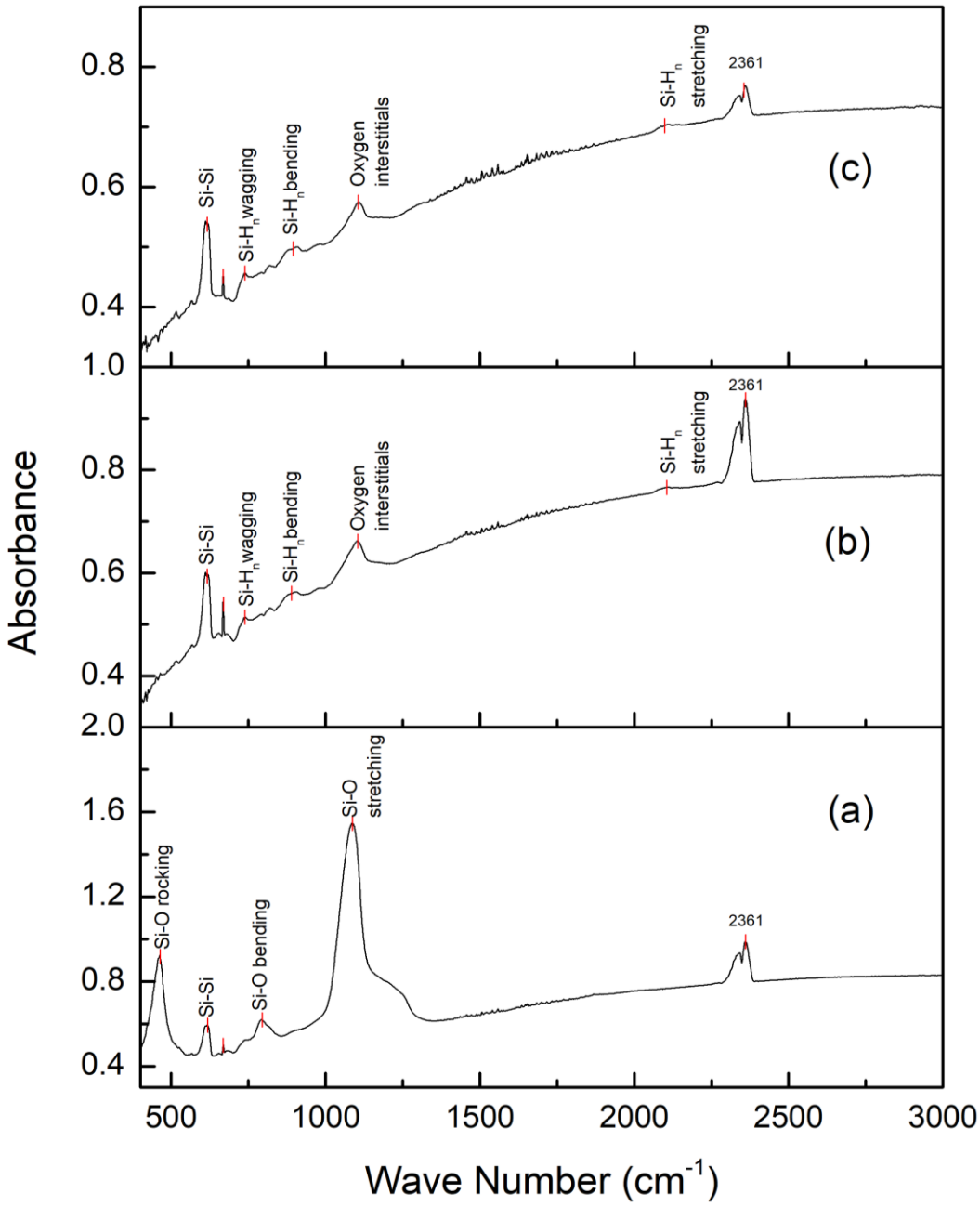

Figure 5-6 Infrared absorption spectra of SiO_2 diatoms sintered into the substrate (a), Si diatoms on a Si-substrate before (b), and after HF etching (c). Residual SiO_2 in (b) was dissolved using HF(c). The peaks at around 2300 cm^{-1} and at 699 cm^{-1} correspond to CO_2.

The completion of the magnesiothermic conversion was confirmed by EDX spectroscopy (Fig. 5-7). After the selective magnesia dissolution, there was a trace of oxygen with silicon as the majority element (Fig.5-7b). After HF etching, the only element that remained in the sample was silicon, while the trace oxygen was removed (Fig. 5-7d). Moreover, after the conversion, the nano-micro pores of the diatoms were preserved (Fig. 5-7a and Fig. 5-7c).

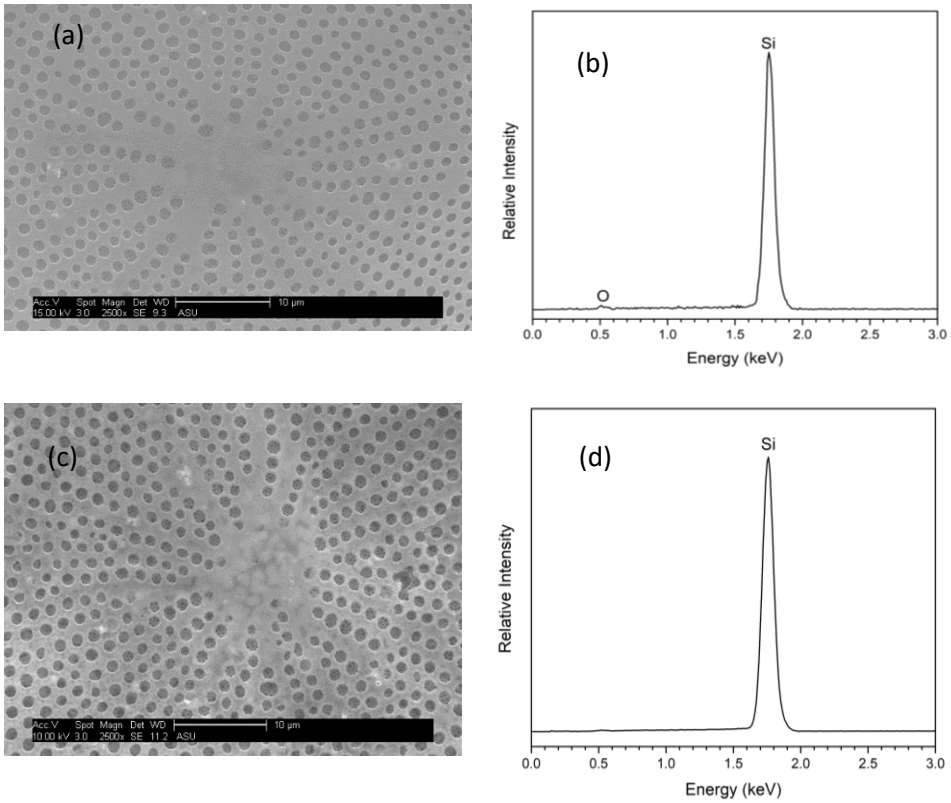

Figure 5-7 Elemental Analysis of the magnesiothermically converted diatoms, sintered into the substrate. After magnesia dissolution (a) and HF etching (c), the nano-micro structures are still preserved. EDX spectra (b) and (d) show elemental composition in (a) and (c) respectively. The spectra confirm the completion of the magnesiothermic conversion as the oxygen was significantly decreased after the conversion (b). The residual SiO_2 in (b) was removed by HF etching as shown in (d)

Interestingly, the sintered diatoms on the silicon wafer survived the magnesiothermic conversion, magnesia selective dissolution, and HF etching. The nano-micro structure of the diatoms was preserved after the conversion and HF etching as shown in Fig. 5-8.

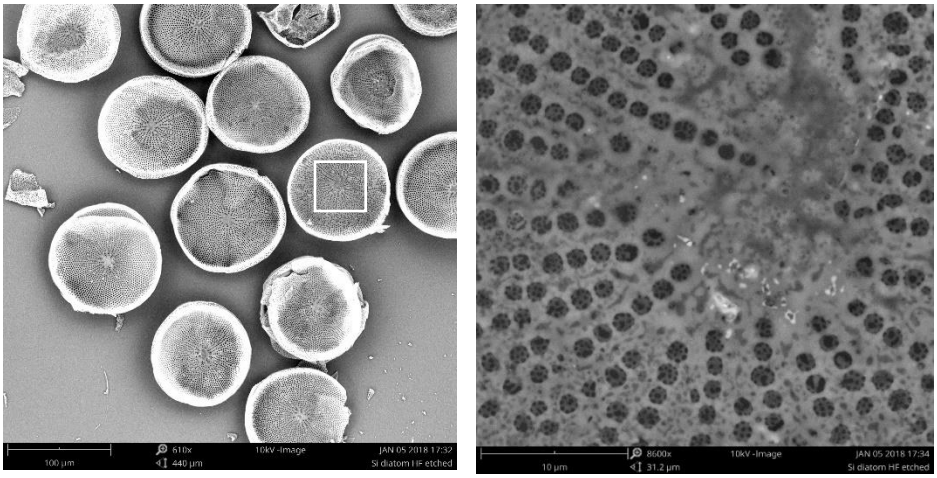

Figure 5.8 Secondary images of Si-diatom on the substrate after HF etching. The nano-micropores of the diatom are observed.

The cross-section image (Fig. 5-9) of the Si-sintered diatom on the substrate reveals that the diatom and the TGO layer become porous after oxygen atoms were removed from the diatom structure by the conversion and HF etching process. The interface image also reveals the preserved areola of the diatoms which survived all the chemical treatment processes. Moreover, the diatoms did not detach from the substrate after the conversion and HF etching though those processes destroy Si-O-Si bonds.

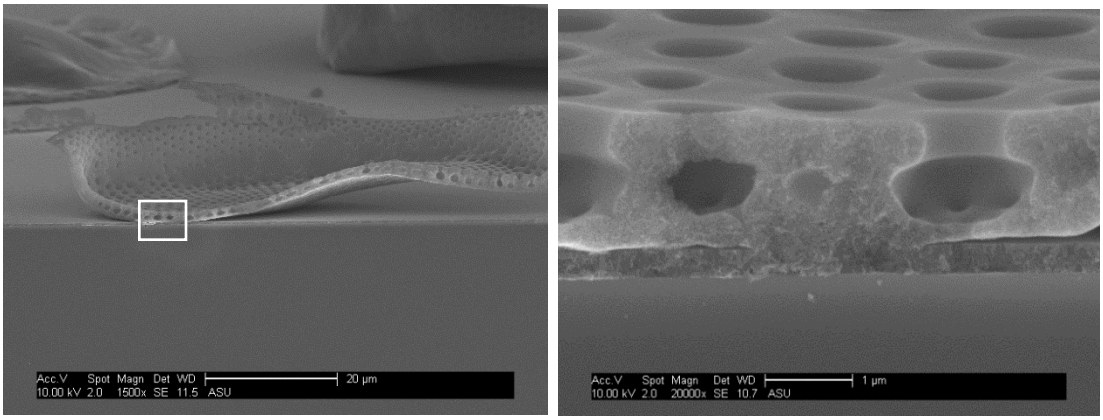

Figure 5-9 Secondary Electron Images of Si-sintered diatom on the substrate (magnesiothermically converted SiO_2 sintered diatoms on the substrate which was sintered at 1125°C). The cross-section images show the porous structure inside the valve and the thin porous Si-layer.

5.3.2 Optical properties of PEDOT:PSS coated Si-diatom monolayer

After the conversion process, the Si-sintered diatoms were spin coated with PEDOT:PSS. The cross-section images (Fig. 5-10) show the homogeneous layer of PEDOT:PSS on the micro-pores of the Si-diatom valve. Though the film did not coat inside the pores, it makes good contact with Si-diatom surface.

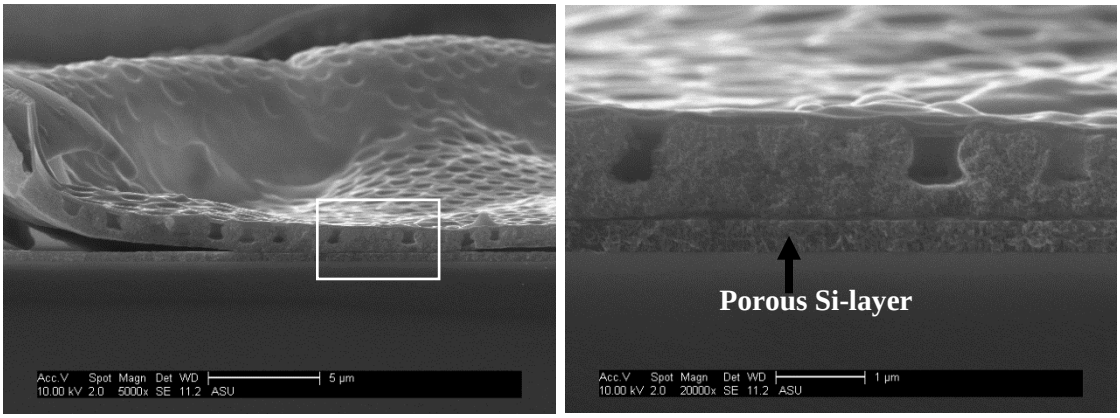

Figure 5-10 Secondary Electron Microscopy images of a PEDOT:PSS layers that was spin-coated on magnesiothermically converted Si-diatoms. The cross-section image indicates that a homogeneous layer of polymer has formed on a Si-diatom.

The optical properties of the modified-diatoms were investigated using visible reflectance spectroscopy as shown in Fig. 5-11. It was found that diatoms sintered on the substrate at high temperatures (SiO_2-sintered diatoms), and magnesiothermically converted sintered substrates without any diatoms (Si-sintered wafer), and magnesiothermically converted SiO_2-sintered diatoms (Si-sintered diatoms) had lower reflectivity compared to a bare silicon wafer (Si-wafer). The spectra of sintered samples also show oscillating behavior due to the different interfaces arising from the SiO_2-TGO layer or porous-Si layer in the magnesiothermic conversion samples. The reflection of light from different interfaces causes constructive (adding intensities) or destructive (subtracting intensities) interference, resulting in intensity oscillation.

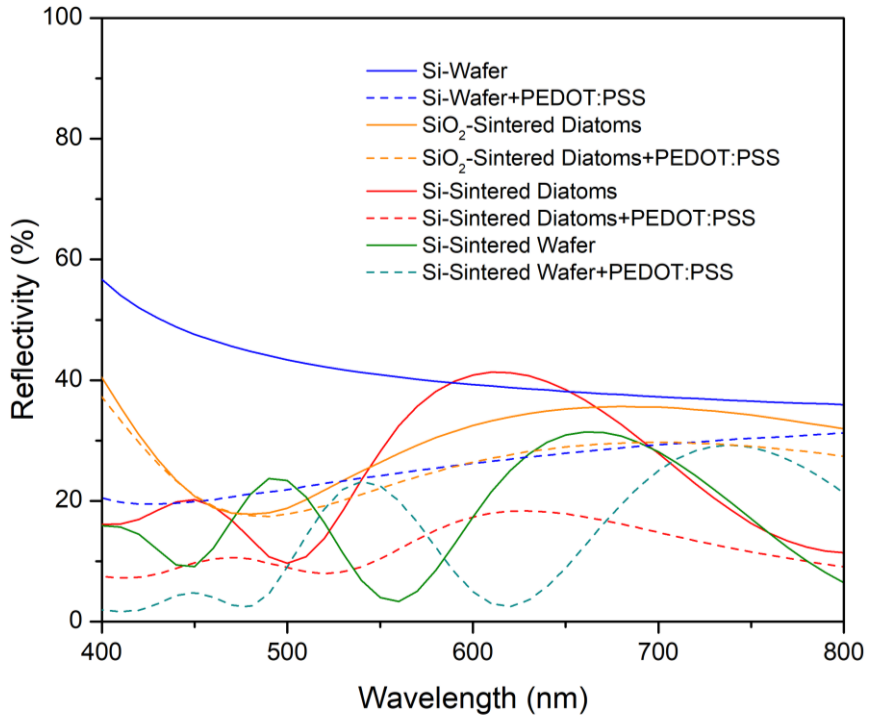

Figure 5-11 Visible reflectance spectra revealing the effects of magnesiothermic converted diatoms (Si-sintered diatoms and SiO_2-sintered diatoms), sintering process (and Si-sintered wafer), and PEDOT:PSS (all dash-line spectra) on light reflectivity

from 400-700nm. The conversion process (Si-sintered diatoms) decreased the reflectivity of the diatoms (SiO_2-sintered diatoms). PEDOT:PSS coating also trended to decrease the reflectivity. Note that the SiO_2-sintered diatom and Si-sintered diatom were from the diatoms which were sintered at 1125°C.

After spin-coating the samples with PEDOT:PSS, the reflectivity of all samples tend to decrease as PEDOT:PSS has an antireflective effect[48]. The PEDOT:PSS also reduced the oscillating behavior of the Si-sintered diatom sample. Additionally, it was found that the PEDOT:PSS coated Si-sintered diatoms show lower reflectivity than PEDOT:PSS coated SiO_2-sintered diatoms and a PEDOT:PSS coated Si-wafer, indicating that the Si-sintered diatoms enhance light absorption over SiO_2-sintered diatoms and a silicon wafer. This suggests that the SiO_2-diatoms need to be converted into Si-diatoms for light harvesting applications. Si-sintered diatoms and a Si-sintered wafer show different reflectivity at different wavelength due to the different oscillating behavior of their reflectance spectra.

It was found in previous studies that a porous silicon layer demonstrated high quantum efficiency[49] and serves as an antireflective coating[50], [51]. Its porous nature makes its reflective index lower than that of bulk silicon[51]. To investigate whether the improved light absorption in Si-sintered diatoms is from the Si-diatoms or the porous-Si layer, the photocurrent of Si-sintered diatoms and a Si-sintered wafer at different wavelengths was measured and reported as the normalized photoresponse as shown in Fig.5-12a. It was found that the differences in photoresponse of the two samples are correlated to the behavior of their reflectivity spectra.

The Si-sintered diatoms exhibit a higher photoresponse at 414 to 467 nm, 475 to 586 nm, and 730-800 nm, at which the reflectance spectrum of Si-sintered diatoms exhibits destructive interference while that of the Si-sintered wafer exhibits constructive interference. In addition, Si-sintered diatoms show lower photoresponse at 467 to 475 nm and 586 to 700 nm, at which the reflectance spectra of Si-sintered diatoms exhibit constructive interference while that of the Si-sintered wafer exhibits destructive interference. The constructive interference in reflectance spectra indicates that the reflectance intensities are added, which implies that less photons were absorbed, resulting in less photocurrent and thus leading to lower photoresponse. Conversely, the destructive interference indicated in the reflectance spectra results in the higher photoresponse.

The enhancement in photoresponse of the Si-diatom structure over the porous-Si layer is shown Fig.5-12b. It demonstrates s that the diatom structure has enhanced the photoresponse over the porous-Si layer at around 414 to 586 nm and 730 to 800 nm, with a maximum enhancement of 44%. This leads to the question whether this enhancement comes from the porous structure inside the diatom caused by the conversion or from the hierarchical structure of the diatom itself. The hierarchical structure of *C.wailesii* exhibited enhanced light absorption efficiency at 400 to 500 nm and 650 to 800 nm, corresponding to the structure of cribrum and areola, respectively[2], [52]. Thus, the enhancement of the Si-diatom structure may come from the hierarchical structure of the diatom itself. The slight shift in wavelength in the two ranges may be due to the shrinkage of the diatom structure during the sintering process as well as the refractive index difference between SiO_2 and Si. Interestingly, although most of the cribellum structure was destroyed during

the sintering process (Fig. 4-6o), the absence of the cribellum does not significantly affect the light absorption since the cribellum structure does not considerably contribute to visible light trapping[52]. The pores in the cribellum structure were smaller than the wavelength of visible light; the scattered field thus was evanescent within the target visible spectrum[52]. At 586 to 700 nm, the porous-Si layer showed higher photoresponse than that of Si-sintered diatoms. Hence, the reflectance and photoresponse measurement demonstrated that, with PEDOT:PSS coating, both diatom structure and the porous-Si layer in Si-sintered diatoms had improved the light absorption for a Si-wafer.

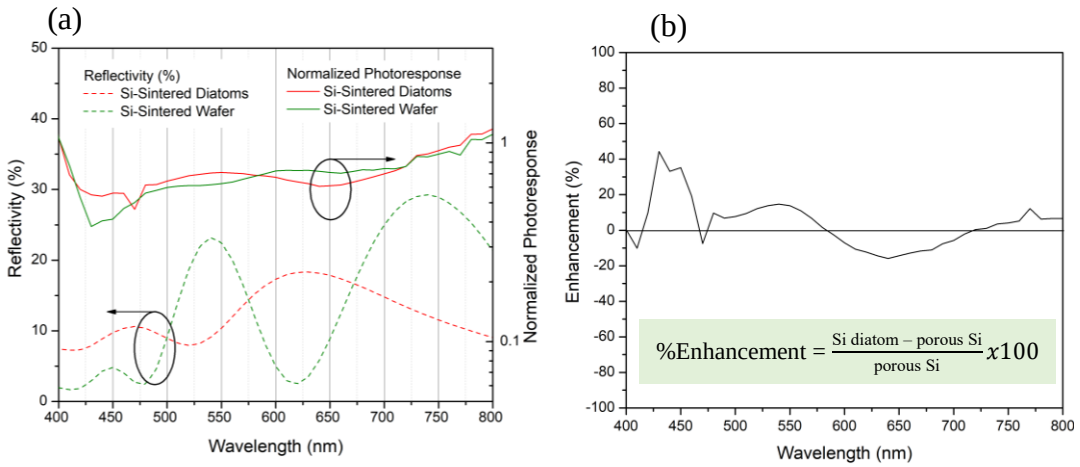

Figure 5-12 Photoresponse of the PEDOT:PSS coated Si-sintered diatoms and Si-sintered wafer from Fig.5-11, compared to their corresponding reflectivity at different wavelength (a). The enhancement of Si-diatoms over the porous-Si layer is shown in (b).

5.4 Conclusion

The SiO_2-sintered diatoms and the TGO layer were magnesiothermically converted into porous Si using magnesium silicide as the magnesium vapor source. The completeness

of the reaction was confirmed by XRD and FTIR. The nano-micro pores, including the areola of the diatom, were preserved after the conversion and HF etching. The PEDOT:PSS coated Si-sintered diatoms show interesting optical properties. According to reflectance spectra, the conversion process and the PEDOT:PSS coating was found to enhance light absorption of the diatoms on the substrate. The photoresponse spectra, which are consistent with reflectance spectra, revealed that the hierarchical structure of the Si-diatoms enhanced light absorption at around 414 to 586 nm and 730 to 800 nm. This is the first time that the diatom *C. wailesii* was directly bonded to the substrate using high temperature, converted into Si, and coated with PEDOT:PSS. This suggests that the PEDOT:PSS/Si-sintered diatoms may be used in light harvesting applications such as solar cells.

REFERENCES

[1] "Diatom," *Wikipedia*. 13-Mar-2018.

[2] Xiangfan Chen, Chen Wang, Evan Baker, Jane Wang, and Cheng Sun, "Understanding the nanophotonic light-trapping structure of diatom frustule for enhanced solar energy conversion: a theoretical and experimental study," 2014, vol. 8958, pp. 89580I-8958–10.

[3] Schmid Anna-Maria M. and Volcani Benjamin E., "Wall morphogenesis in coscinodiscus wailesii gran and angst. i. valve morphology and development of its architecture1," *J. Phycol.*, vol. 19, no. 4, pp. 387–402, Nov. 2004.

[4] Y. Wang, J. Pan, J. Cai, and D. Zhang, "Floating assembly of diatom Coscinodiscus sp. microshells," *Biochem. Biophys. Res. Commun.*, vol. 420, no. 1, pp. 1–5, Mar. 2012.

[5] S. Y. Kwon, S. Park, and W. T. Nichols, "Self-assembled diatom substrates with plasmonic functionality," *J. Korean Phys. Soc.*, vol. 64, no. 8, pp. 1179–1184, Apr. 2014.

[6] J. Cai, X. Wang, A. Li, S. W. Anderson, and X. Zhang, "Biologically enabled micro- and nanostencil lithography using diatoms," *Extreme Mech. Lett.*, vol. 4, pp. 186–192, Sep. 2015.

[7] "Towards uniformly oriented diatom frustule monolayers: Experimental and theoretical analyses | Microsystems & Nanoengineering." [Online]. Available: https://www.nature.com/articles/micronano201664. [Accessed: 29-Mar-2018].

[8] J. Pan *et al.*, "Bonding of diatom frustules and Si substrates assisted by hydrofluoric acid," *New J. Chem.*, vol. 38, no. 1, pp. 206–212, Dec. 2013.

[9] Sumper M. and Brunner E., "Learning from Diatoms: Nature's Tools for the Production of Nanostructured Silica," *Adv. Funct. Mater.*, vol. 16, no. 1, pp. 17–26, Dec. 2005.

[10] M. Sumper, "A Phase Separation Model for the Nanopatterning of Diatom Biosilica," *Science*, vol. 295, no. 5564, p. 2430, Mar. 2002.

[11] Di Caprio Giuseppe *et al.*, “Shedding light on diatom photonics by means of digital holography,” *J. Biophotonics*, vol. 7, no. 5, pp. 341–350, May 2014.

[12] T. Fuhrmann, S. Landwehr, M. El Rharbi-Kucki, and M. Sumper, “Diatoms as living photonic crystals,” *Appl. Phys. B*, vol. 78, no. 3, pp. 257–260, Feb. 2004.

[13] L. D. Stefano, I. Rea, I. Rendina, M. D. Stefano, and L. Moretti, “Lensless light focusing with the centric marine diatom Coscinodiscus walesii,” *Opt. Express*, vol. 15, no. 26, pp. 18082–18088, Dec. 2007.

[14] E. De Tommasi *et al.*, “Multi-wavelength study of light transmitted through a single marine centric diatom,” *Opt. Express*, vol. 18, no. 12, pp. 12203–12212, Jun. 2010.

[15] Shih-Hsin Hsu, Camille Paoletti, Moacir Torres, Raymond J. Ritchie, Anthony W. D. Larkum, and Christian Grillet, “Light transmission of the marine diatom Coscinodiscus wailesii,” 2012, vol. 8339, pp. 83390F-8339–8.

[16] S. W. Boettcher *et al.*, “Photoelectrochemical Hydrogen Evolution Using Si Microwire Arrays,” *J. Am. Chem. Soc.*, vol. 133, no. 5, pp. 1216–1219, Feb. 2011.

[17] S. Chandrasekaran, T. J. Macdonald, Y. J. Mange, N. H. Voelcker, and T. Nann, “A quantum dot sensitized catalytic porous silicon photocathode,” *J. Mater. Chem. A*, vol. 2, no. 25, pp. 9478–9481, 2014.

[18] C. K. Chan *et al.*, “High-performance lithium battery anodes using silicon nanowires,” *Nat. Nanotechnol.*, vol. 3, p. 31, Dec. 2007.

[19] Z. Bao *et al.*, “Chemical reduction of three-dimensional silica micro-assemblies into microporous silicon replicas,” *Nature*, vol. 446, p. 172, Mar. 2007.

[20] Barin, Ihsan and Sauert, Fried, *Thermochemical data of pure substances*, vol. 6940. Weinheim, 1993.

[21] W. Luo *et al.*, “Efficient Fabrication of Nanoporous Si and Si/Ge Enabled by a Heat Scavenger in Magnesiothermic Reactions,” *Sci. Rep.*, vol. 3, p. 2222, Jul. 2013.

[22] S. Chandrasekaran *et al.*, “Silicon diatom frustules as nanostructured photoelectrodes,” *Chem. Commun.*, vol. 50, no. 72, pp. 10441–10444, 2014.

[23] S. Chandrasekaran, T. J. Macdonald, A. R. Gerson, T. Nann, and N. H. Voelcker, “Boron-Doped Silicon Diatom Frustules as a Photocathode for Water Splitting,” *ACS Appl. Mater. Interfaces*, vol. 7, no. 31, pp. 17381–17387, Aug. 2015.

[24] J. Liang, X. Li, Z. Hou, W. Zhang, Y. Zhu, and Y. Qian, “A Deep Reduction and Partial Oxidation Strategy for Fabrication of Mesoporous Si Anode for Lithium Ion Batteries,” *ACS Nano*, vol. 10, no. 2, pp. 2295–2304, Feb. 2016.

[25] Powder Diffraction File Card No. 27–1402 for Si, Card No. 45–946 for MgO, and Card No. 35–0773 for Mg2Si, *International Center on Diffraction Data*.

[26] Ari Gordin, “Shape-Preserving Physical and Chemical Transformations of Si and SiO2 Nano- and Microstructures,” Ph.D. Dissertation, Georgia Institute of Technology, Atlanta, GA, 2014.

[27] Y. Wang, J. Pan, J. Cai, and D. Zhang, “Floating assembly of diatom Coscinodiscus sp. microshells,” *Biochem. Biophys. Res. Commun.*, vol. 420, no. 1, pp. 1–5, Mar. 2012.

[28] D. Losic, J. G. Mitchell, and N. H. Voelcker, “Fabrication of gold nanostructures by templating from porous diatom frustules,” *New J. Chem.*, vol. 30, no. 6, pp. 908–914, Jun. 2006.

[29] “Gold surfaces and nanoparticles are protected by Au(0)–thiyl species and are destroyed when Au(I)–thiolates form | Proceedings of the National Academy of Sciences.” [Online]. Available: http://www.pnas.org/content/113/11/E1424/tab-article-info. [Accessed: 28-Mar-2018].

[30] C. Huwiler, T. P. Kunzler, M. Textor, J. Vörös, and N. D. Spencer, “Functionalizable Nanomorphology Gradients via Colloidal Self-Assembly,” *Langmuir*, vol. 23, no. 11, pp. 5929–5935, May 2007.

[31] F. Silencieux *et al.*, “Mesoporous Silica Nanoparticles under Sintering Conditions: A Quantitative Study,” *Langmuir*, vol. 31, no. 47, pp. 13011–13021, Dec. 2015.

[32] W. Cui *et al.*, “Silicon/Organic Heterojunction for Photoelectrochemical Energy Conversion Photoanode with a Record Photovoltage,” *ACS Nano*, vol. 10, no. 10, pp. 9411–9419, Oct. 2016.

[33] M. Hildebrand, “Biological processing of nanostructured silica in diatoms,” *Prog. Org. Coat.*, vol. 47, no. 3, pp. 256–266, Sep. 2003.

[34] C. E. Hamm *et al.*, “Architecture and material properties of diatom shells provide effective mechanical protection,” *Nature*, vol. 421, no. 6925, pp. 841–843, Feb. 2003.

[35] R. R. L. Guillard and J. H. Ryther, “Studies of Marine Planktonic Diatoms: I. Cyclotella Nana Hustedt, and Detonula Confervacea (cleve) Gran.,” *Can. J. Microbiol.*, vol. 8, no. 2, pp. 229–239, Apr. 1962.

[36] C. Jeffryes, T. Gutu, J. Jiao, and G. L. Rorrer, “Peptide-mediated deposition of nanostructured TiO2 into the periodic structure of diatom biosilica,” *J. Mater. Res.*, vol. 23, no. 12, pp. 3255–3262, Dec. 2008.

[37] Z. Lu and M. Zhou, “Fabrication of large scale two-dimensional colloidal crystal of polystyrene particles by an interfacial self-ordering process,” *J. Colloid Interface Sci.*, vol. 361, no. 2, pp. 429–435, Sep. 2011.

[38] E. Guzmán, L. Liggieri, E. Santini, M. Ferrari, and F. Ravera, “Influence of silica nanoparticles on phase behavior and structural properties of DPPC—Palmitic acid Langmuir monolayers,” *Colloids Surf. Physicochem. Eng. Asp.*, vol. 413, pp. 280–287, Nov. 2012.

[39] “Separation of diatom valves and girdle bands from Coscinodiscus diatomite by settling method | SpringerLink.” [Online]. Available: https://link.springer.com/article/10.1007/s10853-010-4642-x. [Accessed: 28-Mar-2018].

[40] M. G. Nikolaides *et al.*, “Electric-field-induced capillary attraction between like-charged particles at liquid interfaces,” *Nature*, vol. 420, no. 6913, pp. 299–301, Nov. 2002.

[41] A. H. Pakiari and Z. Jamshidi, “Nature and Strength of M−S Bonds (M = Au, Ag, and Cu) in Binary Alloy Gold Clusters,” *J. Phys. Chem. A*, vol. 114, no. 34, pp. 9212–9221, Sep. 2010.

[42] P. Lamoureux, S. Heidemann, and K. E. Miller, “Mechanical Manipulation of Neurons to Control Axonal Development,” *J. Vis. Exp. JoVE*, no. 50, Apr. 2011.

[43] J. R. Szczech and S. Jin, “Mg2Si nanocomposite converted from diatomaceous earth as a potential thermoelectric nanomaterial,” *J. Solid State Chem.*, vol. 181, no. 7, pp. 1565–1570, Jul. 2008.

[44] Y. Wang, P. Shao, Q. Chen, Y. Li, J. Li, and D. He, “Nanostructural optimization of silicon/PEDOT:PSS hybrid solar cells for performance improvement,” *J. Phys. Appl. Phys.*, vol. 50, no. 17, p. 175105, 2017.

[45] “Effect of (3-glycidyloxypropyl)trimethoxysilane (GOPS) on the electrical properties of PEDOT:PSS films - Håkansson - 2017 - Journal of Polymer Science Part B: Polymer Physics - Wiley Online Library.” [Online]. Available: https://onlinelibrary.wiley.com/doi/abs/10.1002/polb.24331. [Accessed: 28-Mar-2018].

[46] S. B. Slama, M. Hajji, and H. Ezzaouia, “Crystallization of amorphous silicon thin films deposited by PECVD on nickel-metalized porous silicon,” *Nanoscale Res. Lett.*, vol. 7, no. 1, p. 464, Dec. 2012.

[47] K. Kajiyama, T. Yoneda, Y. Fujioka, and Y. Kido, “Si-O bond formation by oxygen implantation into silicon,” *Nucl. Instrum. Methods Phys. Res. Sect. B Beam Interact. Mater. At.*, vol. 121, no. 1, pp. 315–318, Jan. 1997.

[48] Y. Sun *et al.*, “Si/PEDOT:PSS Hybrid Solar Cells with Advanced Antireflection and Back Surface Field Designs,” *Nanoscale Res. Lett.*, vol. 11, p. 356, Aug. 2016.

[49] J. P. Zheng, K. L. Jiao, W. P. Shen, W. A. Anderson, and H. S. Kwok, “Highly sensitive photodetector using porous silicon,” *Appl. Phys. Lett.*, vol. 61, no. 4, pp. 459–461, Jul. 1992.

[50] R. J. Martín-Palma, L. Vázquez, P. Herrero, J. M. Martínez-Duart, M. Schnell, and S. Schaefer, “Morphological, optical and electrical characterization of antireflective porous silicon coatings for solar cells,” *Opt. Mater.*, vol. 17, no. 1, pp. 75–78, Jun. 2001.

[51] S. Strehlke, D. Sarti, A. Krotkus, K. Grigoras, and C. Lévy-Clément, “The porous silicon emitter concept applied to multicrystalline silicon solar cells,” *Thin Solid Films*, vol. 297, no. 1, pp. 291–295, Apr. 1997.

[52] X. Chen, C. Wang, E. Baker, and C. Sun, “Numerical and experimental investigation of light trapping effect of nanostructured diatom frustules,” *Sci. Rep.*, vol. 5, p. 11977, Jul. 2015.